GENERALIZED MICROFLUIDIC IMMUNOSENSOR DEVICE FOR ANTIBODY DETECTION

A Thesis

Presented to the Faculty of the Graduate School

of Cornell University

In Partial Fulfillment of the Requirements for the Degree of

Master of Science

by

Aibar Nurmukhanov

August 2016

ABSTRACT

Detection of antibodies is of paramount significance for clinical application for medical diagnosis and treatment of infectious diseases including, but not limited to sexually transmitted infections, tuberculosis, hepatitis, influenza, and haemophilus influenza resulting in thousands of deaths each year.

Here we report fabrication of a generalized microfluidic immunosensor device for antibody detection based on Antibody Catalyzed Water Oxidation Pathway (ACWOP) process. The incorporation of polymer chemistry, optical and soft lithography allows for the creation of a platform comprised of patterned square islands of poly(oligoethylene glycol methacrylate) [POEGMA] polymer brushes surrounded by a photosensitizer and capped with microfluidic channels made of polydimethylsiloxane (PDMS). Our immunosensor will be used for direct antibody detection regardless of antibodies' specificity and type. This research focuses on functionalizing POEGMA brushes with dinitrophenyl ligands for specific adsorption of AlexaFluor®488 labeled anti-2,4-dinitrophenyl (DNP) IgE antibodies.

BIOGRAPHICAL SKETCH

I was born and raised in Kazakhstan. At the age of 18 I decided to continue my college education in the USA. I was admitted to Materials Science and Engineering undergraduate program at the University of Illinois at Urbana-Champaign. During my senior I applied to graduate school in Master of Science in Materials Science and Engineering at Cornell University.

Dedicated to my mama and papa

Thank you for loving me, unconditionally

ACKNOWLEDGMENTS

I would like to thank all the people who helped me on this project: Roselynn Cordero, for helping on polymer brush polymerization of the platform, its functionalization, and electropolymerization of the photosensitizer, Eshan Mitra from Barbara Baird Group for supplying me with fluorescently labeled antibodies and other chemical reagents, necessary for antibodies incubation procedure, also Beth Rhoades for giving me suggestions on SU-8 master mold fabrication as well as Carol Bayles for spending time with me on figuring out appropriate acquisition parameters for Confocal Microscopy Imaging. Finally, I would like to thank my principal investigator, professor Christopher K. Ober for giving me an opportunity to work on a biosensor project and helping me to make my stay at Cornell University more enjoyable.

Last but not least, I would like to thank my parents for unconditional love and support as well as my friends that I made my experience at Cornell University unforgettable.

TABLE OF CONTENTS

LIST OF FIGURES

CHAPTER 1

CHAPTER 2

CHAPTER 3

LIST OF TABLES

CHAPTER 1

The use of optical lithography and polymer brush chemistry in generalized platform fabrication for antibody detection

Abstract

Immunosensors are analytical solid-state devices in which the biological reaction (antibody-antigen interaction) is linked to a transducer, which then converts it to a signal. The fundamental advantage of all immunosensors is the molecular recognition at faster times and lower costs as opposed to conventional methods such as polymerase chain reaction or enzyme-linked immunosorbent assay that must be operated by well-trained technician[1-2].

This chapter focuses on the fabrication and characterization of the platform with two different surfaces by photolithography, polymerization with POEGMA brushes by Atom-Transfer Radical Polymerization (ATRP) and electropolymerization of $[Ru(v\text{-}bpy)_3](PF6)_2$, where v-bpy is 4-vinyl, 4'-methyl bipyridine, photosensitizer on fused silica and gold surfaces, respectively. Finally, brushes were functionalized with dinitrophenyl groups for specific binding of fluorescently labeled (AlexaFluor®488) anti-DNP IgE antibodies, which was confirmed by Confocal Microscopy.

Introduction

Infectious diseases still inflict long-standing global health problems, especially in developing countries, causing millions of deaths worldwide. One of the earliest pandemics known to humans was the Black Death during the fourteenth century resulting in at least 50 million deaths with some estimates as high as 200 million. Another example of a devastating infectious disease that caused at least 40 millions of deaths worldwide is 1918 Spanish Flu between 1918-1919 and nearly 675,000 people died in the United States just in that short period of time. The reasons for these highly destructive pandemics remain unknown up until now. One the recent and the largest outbreaks of infection disease was Ebola Virus Disease in West Africa during 2014 year that took away 11,000+ human lives. On the other hand, according to the Centers for Disease Control and Prevention more than 71% of total cases have survived Ebola thanks to collaborative work of thousands of experts from more than 120 countries who made substantial progress in fighting back the virus outbreaks[3-10].

For most infectious diseases laboratory-based tests with acceptable sensitivities and specificities already exist and many lives of infected patients could be easily saved if diagnosed and treated in time. However, many places in the world like West Africa often lack sophisticated clinical facilities, well-trained personnel and expensive chemicals for reliable diagnostic tests to ensure proper patient monitoring. Therefore, simple and inexpensive detection devices that require comparatively simple equipment and could be done in a short amount of time with reliable results are on the hot topic for many researchers.

One of the early markers for infectious diseases is the presence or the absence of antibodies. In the case of infection, non-self substances (toxins) also known as antigens enter a human's body and then that person's immune system generates millions of new B cells that

circulate throughout our body. These B cells randomly create various kinds of antibodies to attach to toxin molecules and inactivate them. Then, antibodies bound to the surface of antigens communicate with other protective cells to come and destroy foreign substances. This type of response is called the humoral immune response also known as the antibody response[11-15].

The goal when treating infected patients is to stimulate this type of response by injecting an agent that can mimic a virus in the weakened form of the microorganism and stimulate the body's immune system to recognize it, so that later it will provide a defense against a real infection. For that reason, effective and rapid diagnostic tests in the form of immunosensors are essential for early detection, disease control, vaccine invention and avoidance of long-lasting complications[16-17].

In this chapter, a generalized biosensor's platform was fabricated based on the Antibody Catalyzed Water Oxidation Pathway (ACWOP) process using conventional optical lithography, lift off process, metal deposition by e-beam evaporation, polymerization of POEGMA brushes and its functionalization with hapten groups for specific binding of antibodies. A work done by Wentworth et al. (2006) showed that all antibodies catalyze the reaction between singlet dioxygen and dihydrogen monoxide to produce electrochemically detectable hydrogen peroxide given the certain chemistry. In the ACWOP process, the idea is to produce singlet dioxygen, which is generated from interaction between ambient oxygen and photosensitizer upon UV irradiation. Ober and coworkers used Square Wave Voltammetry (SWV) to measure the mole ratio of hydrogen peroxide generated per antibody through an electrochemical reduction of red-fluorescent product, resorufin, which was originated from the reaction between hydrogen peroxide and Amplex Red in a 1:1 in the presence of horseradish peroxidase. The mole ratio of hydrogen peroxide per antibody is heavily affected by the presence of photosensitizer in close

proximity to the functionalized POEGMA brushes. They have shown that hydrogen peroxide at concentrations as low as 0.33 nM can be detected using this approach.

Finally, the ACWOP process was compared to more popular detection methods based on enzyme-linked immunosorbent assay (ELISA) in more details. The idea behind the ACWOP implemented in our immunosensor device is depicted in Figure 1[18-19].

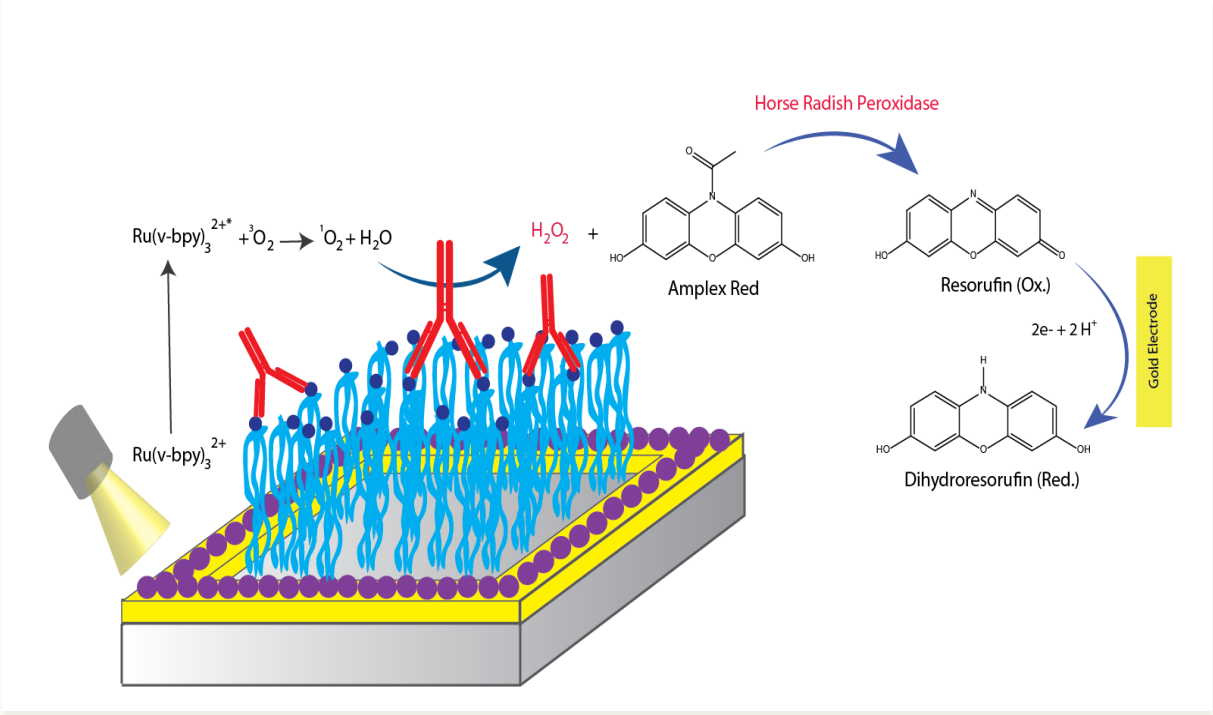

Figure 1. The illustration of generalized immunosensor platform based on the ACWOP process. Polymer brushes are grown from the substrate (grey surface), and photosensitizer (purple spheres) is electropolymerized on gold lines (yellow surface). Hapten groups (dark blue spheres) are responsible for specific recognition and binding to antibodies (Y-shaped red symbol)

EXPERIMENTAL SECTION

Platform fabrication via contact optical lithography

A patterned device, consisting of 35 rows of seventeen fused silica squares (300x300 μm) surrounded by a patterned gold lines (150 μm wide) was fabricated using lift-off process. Lift-off process includes spin coating a bilayer of photoresists: lift-off resist LOR 10A (based on polydimethylglutarimide) and positive-tone SPR220-3.0 photoresist (based on cresol novolak resin and diazo photoactive compound) on fused silica substrate followed by baking at 180 ^{o}C for 3 minutes and 115 ^{o}C for 1.5 minutes, respectively. An ABM contact aligner with mercury arc lamp (i-line: 365 nm optical source) was used to expose a positive photoresist for 10 seconds followed by post-exposure bake at 115^{0}C for 1.5 minutes. Then, the substrate was developed by Hamatech-Steag Wafer Processor using a double puddle automated process in tetramethylammonium hydroxide (TMAH) solution to obtain an undercut profile for metal deposition. Subsequently, 15 nm of chromium (adhesion layer) and 100 nm of gold layers were deposited on the wafer using a CVC SC4500 electron beam evaporation system. A solution of Remover 1165 was used remove photoresist and obtain isolated pattern of gold lines as shown in Figure 2. The whole wafer was cut into six individual platforms using all-purpose blade on DISCO-dicing saw. The same positive photoresist (SPR220-3.0) was spin-coated on the wafer as a sacrificial layer before dicing. All photolithography steps are outlined in Table I.

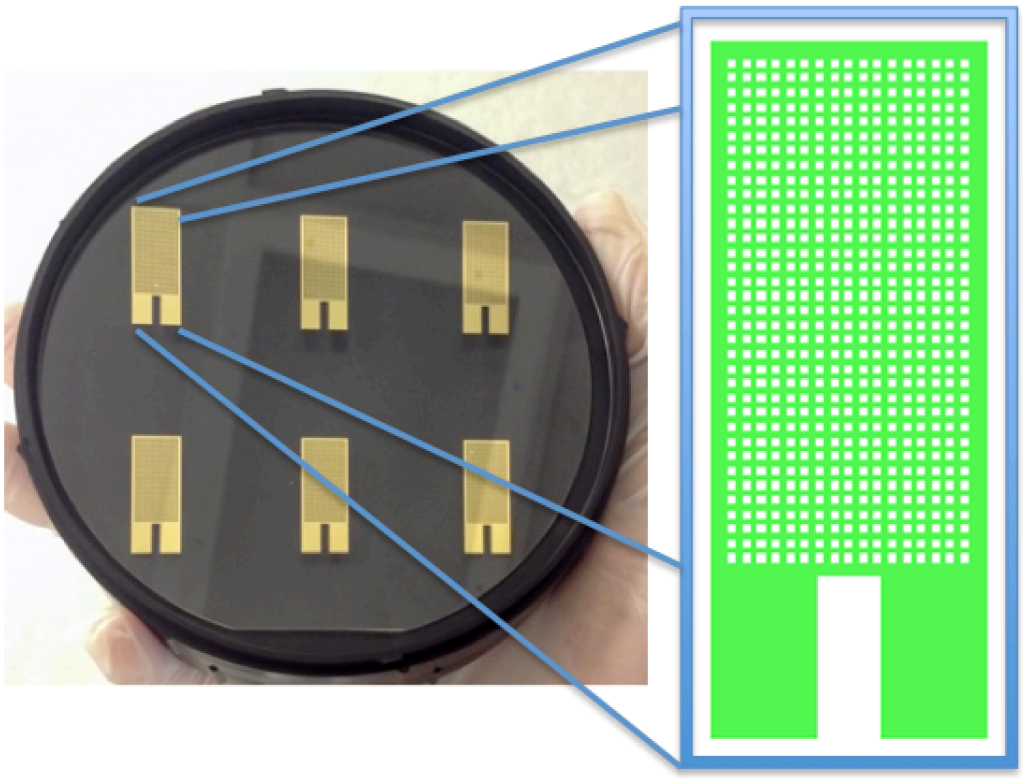

Figure 2. Lift-off process and electron gun metal evaporation system were used to create a 2.15 cm x 0.85 cm platforms with contact pads on fused silica wafer with patterned lines of gold (green area)

TABLE I. Step-by-step platform fabrication process via photolithography

1) Place onto hot plate @ 180 ^{0}C for 20 min (for dehydration, uniformity) **- Spin LOR 10A, 3000 rpm (10, 000 rpm/s) for 1 min** **- Bake @ 180 ^{0}C, 3 min**
2) Spin SPR220-3.0, 4000 rpm (4krpm/s) for 1 min **- Bake @ 115 ^{0}C, 1.5 min**
3) Soft contact Exposure for 10 sec **- Post exposure Bake at @ 115 ^{0}C for 1.5 min**
4) Developing via Hamatech-Steag Wafer Processor **- Using 726 MIF 90 sec DP program**
5) O_2 descum via Anatech Resist Strip **- 1 minute (150 Watts)**
6) Electron-beam metal evaporation **-15 nm of chromium (adhesion layer) and 100 nm of gold**
7) Soak in 1165 remover for lift off (repeat at least 2 times for 2 hours each) **-Rinse in acetone, DI water, and isopropanol and dry with nitrogen gun.** **8) Spin SPR220-3.0 4000 rpm for 60 sec (4000 rpm/sec), Bake @ 90 ^{0}C for 0.5 min (protection layer)** **9) Cut wafer using dicer with all-purpose blade**

Polymerization of POEGMA by Atom-Transfer Radical Polymerization

Two fused silica platforms (2.15 cm x 0.85 cm) were placed in a Schlenk flask. Poly(oligo ethylene glycol methacrylate) [6.61 g], CuCl (19.5 mg), $CuBr_2$, (4.30 mg), and 2,2'-bipyridine (76.0 mg) were added to another Schlenk flask containing a magnetic stir bar. Both flasks' water vapor and air were replaced with nitrogen at least three times. Deionized water (10.0 ml) was purged with nitrogen gas for 25 minutes and then transferred to the Schlenk flask carrying the monomer via cannula, preventing atmospheric contamination. The solution was stirred under nitrogen gas and transferred into the flask containing the platforms. Polymerization was done at room temperature for 8-15 minutes, after that platforms were washed with water/ethanol, dichloromethane (DCM) and dried with nitrogen gun. Same procedure was used to grow polymer brushes on silicon wafer.

POEGMA brushes were also polymerized on silicon wafer using similar method for characterization purposes via ellipsommetry for thickness measurements. In ellipsometry, reliable thickness measurements can only be measured on a non-transparent substrate. In the case of transparent substrates such as fused silica, additional reflections from the back surface take place which affects the spectra acquired by the tool. Ellipsometry confirmed thickness measurements to be around 10 nm for POEGMA brushes on silicon wafer.

Functionalization of POEGMA brushes with 2,4-dinitrophenyl (DNP) groups.

A solution mixture of dinitrophenyl-ε-amino-n-caproic acid (37.5 mg), *N,N′*-diisopropylcarbodiimide (DIPC) [125 μL], and 4-(dimethylamino)pyridinium-4-toluene sulfonate (DPTS) [188 mg] in anhydrous dimethylformamide (DMF) [10 ml] were transferred into the flask containing the platforms via cannula to react for 24 hours at 32 ^{0}C. Platforms were washed with water/ethanol and dried with nitrogen gun. Synthesis of polymer brushes and their subsequent functionalization is illustrated in Figure 6.

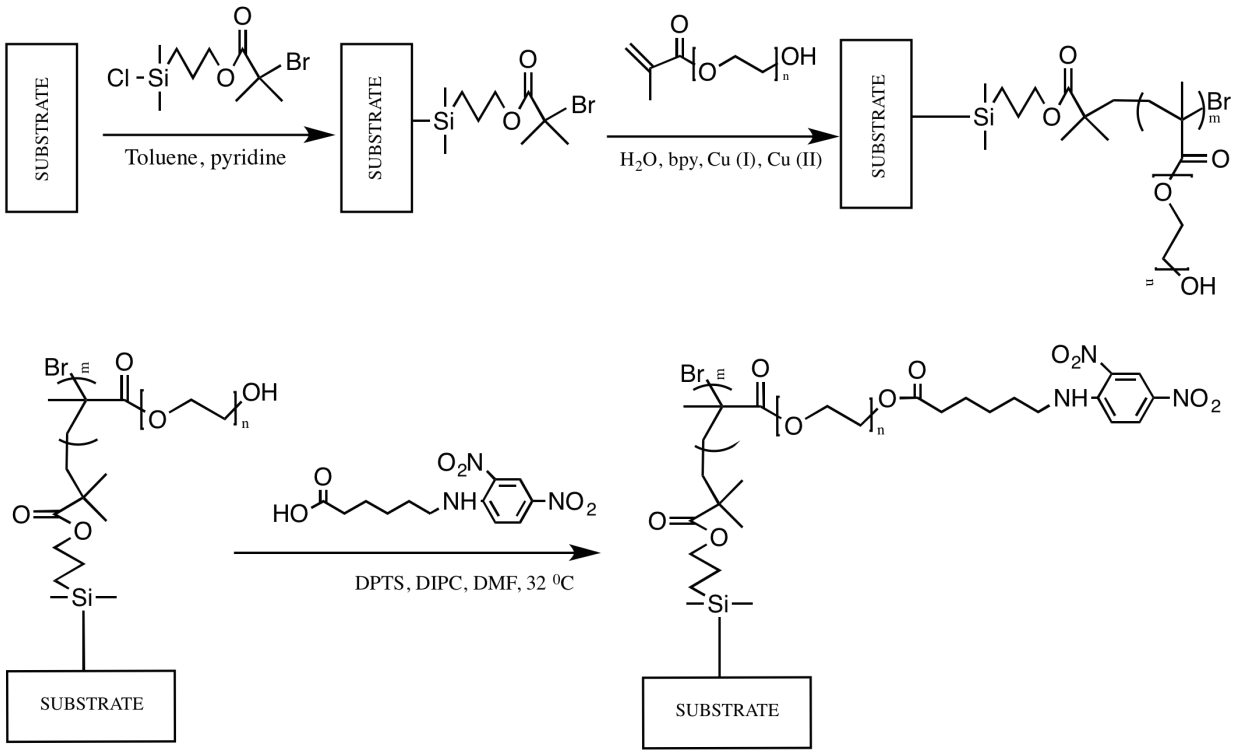

Figure 3. Synthesis of POEGMA polymer brushes on a platform and their functionalization with 2,4-dinitrophenl (DNP) groups for specific binding to fluorescently labeled anti-DNP IgE antibodies

Electrochemical polymerization of $[Ru(v\text{-}bpy)_3](PF6)_2$ photosensitizer

The gold-plated quartz crystal was submerged in 0.5 nM solution of tris(2,2′-bipyridine)ruthenium(II) hexafluorophosphate**,** $[Ru(v\text{-}bpy)_3](PF6)_2$ where v-bpy is 4-vinyl-4'-methyl-2,2'-bipyridine in 0.1 M tetrabutylammonium perchlorate in acetonitrile (0.1 M $TBAPF_6$ /MeCN), and the nitrogen was purged into solution to repalce oxygen. A coiled platinum wire and a silver wire were used as the counter and reference electrodes, respectively. The potential was cycled for several cycles at a sweep rate of 100 mV/s. With increasing number of cycles current also increased proving that layer of electroactive photosensitizer formed on the electrode upon reduction. Finally, the electode was taken out and rinsed with acetone and acetonitirle, and then re-immersed in fresh electrolyte solution[20].

RESULTS AND DISCUSSION

The design of the platform was built in such a way in order to utilize the idea behind the ACWOP process described above and maximize the amount of hydrogen peroxide generated per antibody, i.e. improve the sensitivity of the immunosensor. Therefore, squared islands of fused silica surface fabricated via photolithography and lift-off process were polymerized with POEGMA brushes and surrounded with enclosed pattern of photosensitizer, tris(2,2′-bipyridine)ruthenium(II) hexafluorophosphate, by electrochemical deposition on a gold surface.

In order to promote adhesion between fused silica and Au, chromium was used as an adhesion layer. The chromium is an oxygen active material and acts as a nucleation center, leveling out the topography and decreasing the roughness of the surface of the polycrystalline glass prior to Au deposition. Experiments conducted on evaporating Au on glass (corning glass substreate 7039) revealed that roughness of the polycrystalline surfaces (20 nm in height and 100

nm in lateral extension) decreased to less than 4 nm (lateral extension) by using chromium as a sacrificial layer[21].

One of the challenges associated with Au deposition is the gold spitting. Spitting is the result of several parameters such as deposition rate, deposition power and crucible type. If evaporated rapidly, the power density reaches a critical value and boiling of the gold near the surface occurs - gold nodule defects. Nodule defect is the creation of various sized particles that could result in the electrial short circuits and damage future immunosensor device. Evaporating at slower rates and power partially reduces the issue but not completely, it was shown by Kezia Cheng that spitting increases with carbon count level in the source. Carbon reduces the effective beam area while raising the deposition power requirement for any given metal evaporation rate. This correlation is also known as power density. In order to better maintain the power density below its critical value, gold sources need to be conditioned prior to deposition by removing carbon residuals. K. Cheng showed that even fresh gold pellets always have carbon residuals trapped in layers. Conditioning requires evaporation of metal for at least 5 minutes before opening the shutter and depositing gold on the surface of the wafer. Finally, after the lift-off process it's important to prevent re-attachment of gold particles on the surface of the substrate, by placing wafers face down in MICROPOSIT^{TM} REMOVER 1165 solution (based on mostly 1-methyl-2-pyrrolidinone), rinsed multiple times in acetone, deionized (DI) water, isopropanol, and dried with nitrogen gun[22].

Our immunosensor device also consists of patterned POEGMA polymer brushes polymerized on fused silica glass substrate using atom transfer radial polymerization. POEGMA brushes were are known to be resistant to protein adsorption. In the work done by Sascha Herrwerth and co-workers, self-assembled monolayers with oligo(ethylene glycol) tail on gold

showed strong protein repellant properties due to the inner hydrophilicity, lateral packing density, and ability of the water to penetrate through the self-assembled monolayers to achieve high resistance to protein adsorption. Penetration of the water into the self-assembled monolayers can be challenging therefore requires optimization of lateral packing density. This resistance also depends on other interaction forces such as hydrophobic, van der Waals attraction, steric repulsion and etc. However, the net force depends mainly on the thickness of the grafted polymer rushes and their surface coverage[23-24].

These POEGMA brushes were functionalized with dinitrophenyl ligands for highly specific and sensitive antibody based system where anti-DNP IgE antibodies bind to polymer brushes in a controlled way. According to previous research, immobilization of the monoclonal anti-DNP IgE antibodies happens in a two-step model: monovalent and covalent attachment. Ober and co-workers have shown that on average for every IgE bound to the surface about twenty 2,4-dinitrophenyl groups are screened assuming a rough estimation of the ratio between the binding surface area and area per ligand. Moreover, apparent affinity constant was determined to be around 10^8 M^{-1} for two-step binding process[25].

Electropolymerization of ris(2,2′-bipyridine)ruthenium(II) hexafluorophosphate**,** [Ru(v-bpy)$_3$](PF6)$_2$ on the gold surface (typical coverage of the photosensitizer under conditions described in the experimental section results in the film thickness of roughly 20 nm) and next to the POEGMA brushes, maximizes the production of hydrogen peroxide (Ober et al., 2014). Hydrogen peroxide is generated via reaction between water and singlet oxygen. Singlet oxygen is the product of the reaction mechanism triggered by irradiation of the photosensitizer with UV (~1 hour) from ambient oxygen. The production of singlet oxygen adjacent to the antibody enhances the signal-to-noise ratio as well as the sensitivity of the ACWOP-based immunosensor.

In the presense of horseradish peroxidase, 10-acetyl-3,7-dihydroxyphenoxazine (Amplex® Red reagent) reacts with hydrogen peroxide in a 1:1 stoichiometry to produce resorufin, which can be reduced to dihydroresorufin at the electrode. It was measured by Welch and co-workers that the ratio of hydrogen peroxide generated per IgE antibody was in the range of 640-1200 and that electropolymerization of photosensitizer should take place near POEGMA brushes for improved sensitivity and more efficient hydrogen peroxide generation[25-29].

Other details of the platform design include: the outermost wall (500 μm wide) that provides a pathway for current distribution and ensures uniform polymerization of photosensitizer throughout the whole area of the device, contact pads for electrical connection via crocodile clips, and checkerboard pattern for implementing the idea of the ACWOP in our immunosensor device. Number of rows and columns of squared islands of fused silica were optimized in such way to fit them nicely inside the platform (2.15x0.85 cm).

The lift-off process was chosen to fabricate contact pads and checkerboard pattern because it creates a "line-of-sight" deposition to produce isolated pattern and prevents undesirable "fencing" issues, i.e. material build-up at the edges of the pattern after lift-off process. Double layer of photoresist: SPR220-3.0 (based on polydimethylglutarimide) and LOR 10A (based on cresol novolak resin and diazo photoactive compound) creates undercut profile for further metal deposition. Since e-beam deposition is anisotropic process the amount of resist undercut is not as critical to achieve isolated pattern of gold layers wihout the fencing or the flagging issues[30].

CHARACTERIZATION OF THE PLATFORM

Surface characterization of the platform by contact profilometer with 1mm scan length confirmed the step height, width, and pitch size of the pattern to be around 121 nm, 300 μm, 450 μm, respectively (Fig. 3).

For surface characterization of the POEGMA brushes, a high resolution Atomic Force Microscopy (AFM) was used to measure the thickness of the polymer brushes on two different substrates: fused silica and silicon wafer. In order to measure step height using tapping mode AFM, measurements were performed only on pure fused silica or pure silicon wafer surfaces without gold patterns. A scalpel was used to make several scratches at different points on the substrate by cutting through the polymer brushes. Depending on the thickness, downward pressure on the blade should be applied very carefully to avoid penetration through the glass. An AFM scan is performed around the edge of the scratch to reveal a profile of the surface. For both substrates, POEGMA brushes were measured to be 8-9 nm thick (Fig 4-5). It's important to note, that penetration through the brushes with a blunt instrument leaves contamination of the polymer brushes near the edges of the scratch, resulting in the peak in the AFM scan which was neglected for thickness measurements.

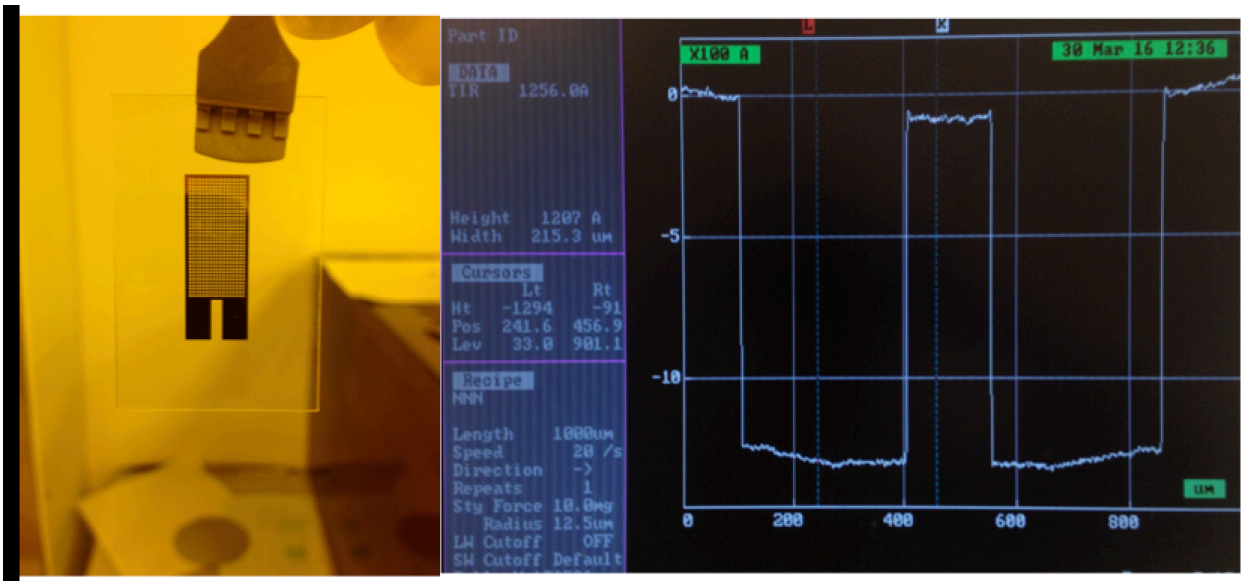

Figure 4. Surface characterization of the platform by P10 Profilometer2 metrology tool (Cornell NanoScale Science and Technology Facility). Output parameters include step height, width, and pitch size of the pattern to be around 121 nm, 300 µm and 450 µm, respectively

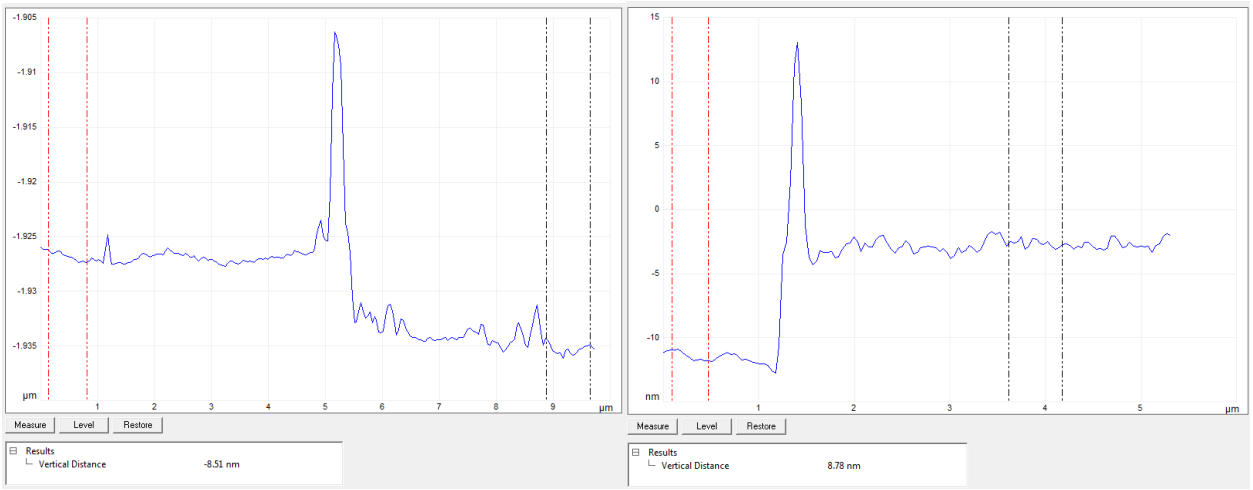

Figure 5: Tapping mode high-resolution surface profilometry measurements of polymer brushed modified fused silica substrate by Veeco Icon Atomic Force Microscope. POEGMA brushes' thicknesses were measured to be around 8-9nm

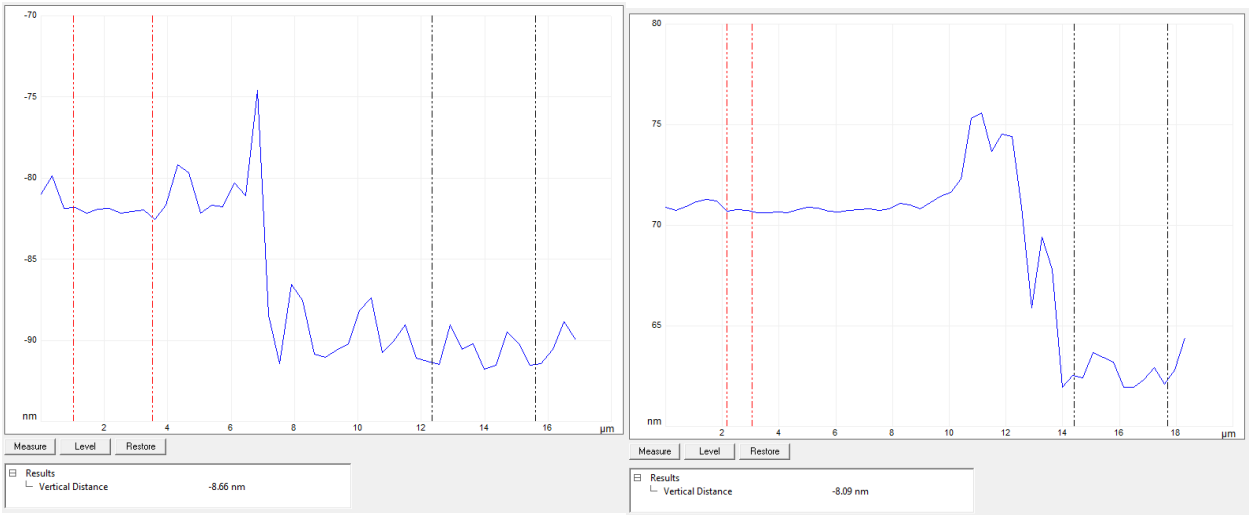

Figure 6: Tapping mode high-resolution profilometry measurements of polymer brushed modified silicon wafer by Veeco Icon Atomic Force Microscope. POEGMA brushes' thicknesses were measured to be around 8-9nm

Functionalization of POEGMA brushes with dinitrophenyl ligands were confirmed by incubating AlexaFluor®488 labeled anti-DNP IgE antibodies. Antibodies were incubated on top of the platform following by standard procedure using buffer solution and bovine serum albumin to prevent non-specific attachment of antibodies to the device for 1 hour in the dark. More specifically, two different samples with POEGMA brushes grown on the fused silic surface: functionalized with DNP and no functionalization were tested using a confocal Microscope under the same acquistion parameters. One of the samples was scratched with a scalpel for AFM characterization before antibody incubation and showed clear difference in fluorescence while second sample showed no fluorescence (except for background fluorescence) (Fig. 7)[31-33].

A) 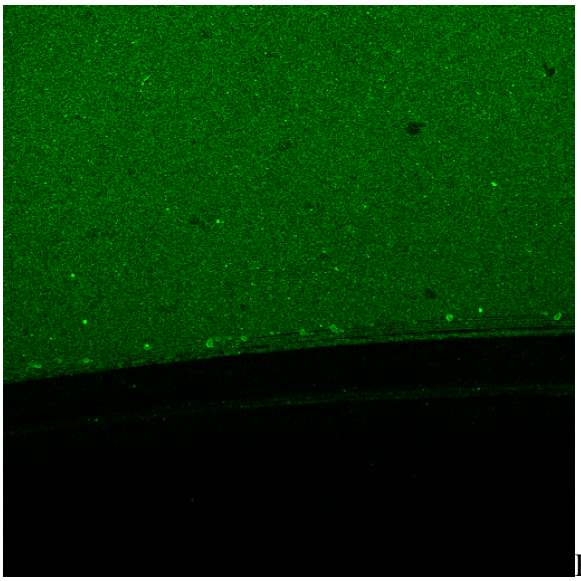 B) 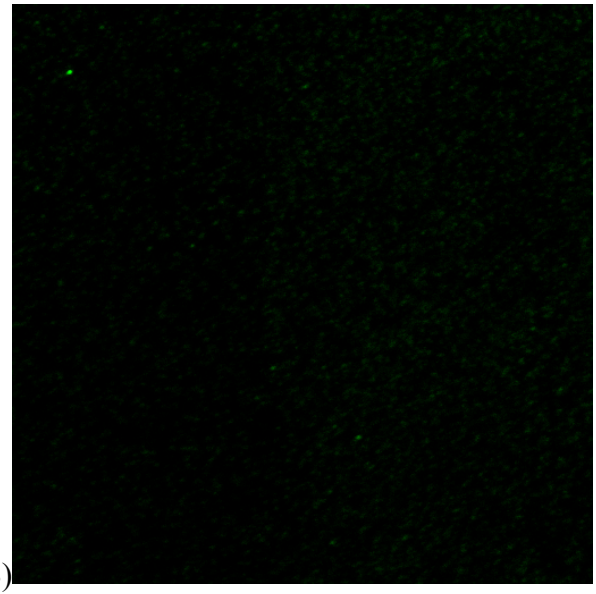

Figure 7. Specific binding of fluorescently labeled (AlexaFluor®488) anti-DNP IgE to POEGMA brushes conjugated with dinitrophenyl groups (A) and not conjugated (B). Little to no (mean GV = 1276) fluorescence above background fluorescence level (mean GV = 642) was measured/observed on surfaces without DNP groups under the same antibodies incubation and image acquisition conditions.

Finally, electropolymerization of our photosensitizer was confirmed by Square Wave Voltammetry using QCM crystal containing polymer brush silane initiator. Potentials were calibrated and then cycled for several cycles at a sweep rate of 100 mV/s. With increasing number of cycles currect also increased. This is due to the fact that that layer of electroactive photosensitizer formed on the electrode upon reduction (Fig. 8). Finally, the electode was taken out and rinsed with acetone and acetonitirle, and then re-immersed in fresh electrolyte solution (Fig. 9).

The idea behind the ACWOP process integrated in our immunosensor compares favorably to the most widely used methods for detecting antibodies based enzyme-linked immunoseorvent assay (ELISA). There are also different types of ELISA which include direct, indirect, sandwich, competitive and other methods of detection. Direct ELISA is a rapid detection mechanism which doesn't require secondary antibody conjugate for antibody detection, however labeling of the each specific ELISA system is slow and often results in weak signal. In our immunosensor signal can be enhanced by implementing different types of photosensitizers in close proximity with POEGMA to generate singlet oxygen adjacent to immobilized antibodies, therefore improving the sensitivty of the immunosensing device.

Indirect ELISA is a more sensitive method compared to direct ELISA due to the fact that multiple labeled antibodies are attached to the primary antibody; however, a secondary antibody or antigen may introduce non-specific attachnment of antibodies leading to false positives or false negatives. In addition, indirect ELISA even though it is more popular method, it requires additional procedural steps that needs to be taken into account.

For ELISA-based detection methods, noise to signal ratio is another challenge which is minimized in our case by blocking a non-specific binding of antibodies using poly(oligoethylene

glycol) units and BSA solution, described above. Finally, our immunosensor platform can be integrated with microfluidics for analyzing and detecting multiple samples simultaneously. In addition, integration of microchannels with the platform can be used in working and analyzing small sample volumes, on the order of few microliters.

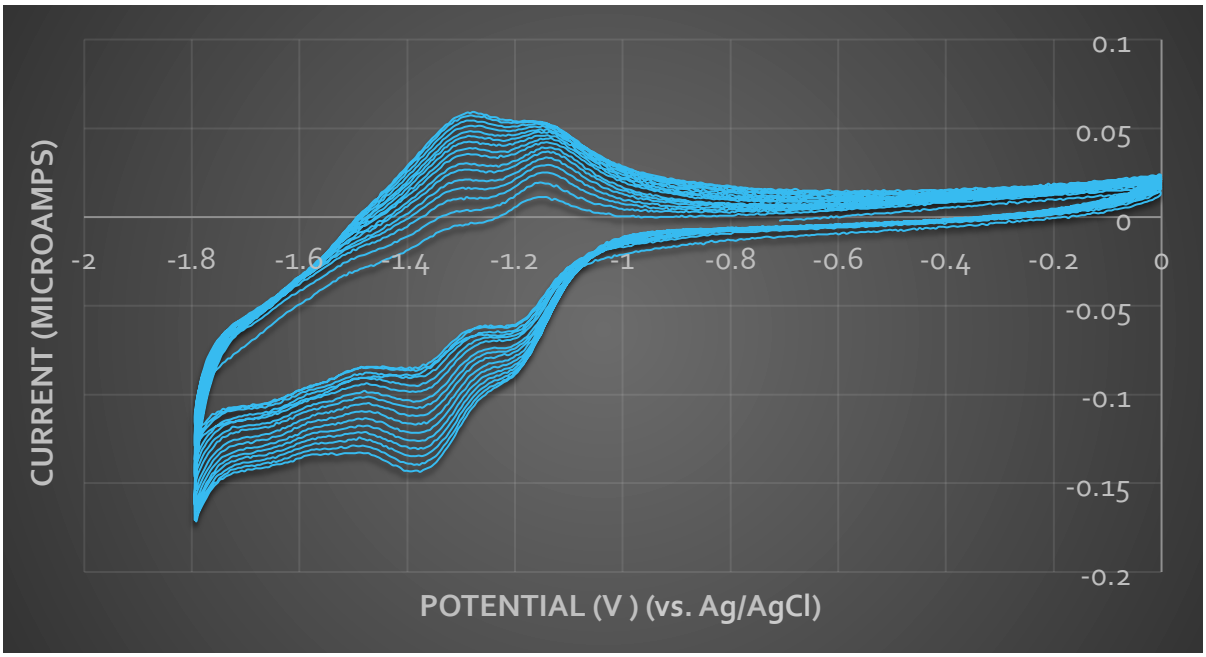

Figure 8. Cyclic voltammmograms of photosensitizer for quartz crystal platforms submerged in 0.5 mM $[Ru(v\text{-}bpy)_3](PF6)_2$, confirming electropolymerization via reduction on Au disk electrode. Multiple lines represent increasing number of cycles.

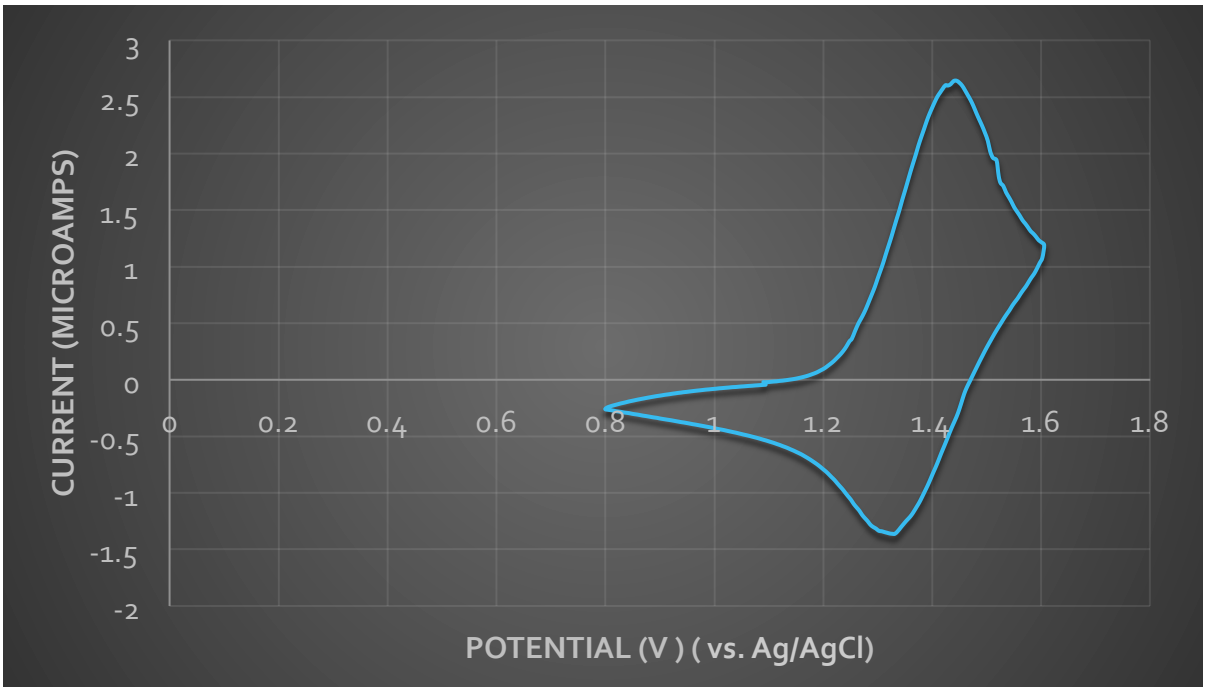

Figure 9: Cyclic voltammmogram of photosensitizer for an electropolymerized layer of $[Ru(v\text{-}bpy)_3]^{2+}$ on Au disk electrode in blank solution.

Conclusion

In this chapter, it was shown that the ACWOP process could be successfully integrated in the immunosensor device, by fabricating a platform with specific design including different surfaces, contact pads and features with specific dimensions and geometries to accommodate poly(oligoethylene glycol) methacrylate brushes on fused silica surface and tris(2,2′-bipyridine)ruthenium(II) hexafluorophosphate, $[Ru(v\text{-}bpy)_3](PF6)_2$ photosensitizer on gold surface. Two different surfaces (gold patterns on fused silica) were fabricated using lift off process, metal deposition by e-beam evaporation, and photolithography. The platform's surface was characterized by contact profilometry for measuring the thickness, the width and the pitch size of the patterned features. Furthermore, successful polymerization of POEGMA brushes with protein resistant properties of the oligoethylene glycol moieities on fused silica surface was successfully achieved by atom transfer radical polymerization. Thickness of POEGMA brushes was characterized and measured using tapping mode AFM and scratching through polymer brushes with a scalpel. On average, POEGMA brushes polymerized on fused silica surface were 8 to 9 nm tall. Then, POEGMA brushes were functionalized with 2,4-dinitrophenyl groups based on two-step binding process of anti-DNP IgE antibodies. These antibodies were fluorescently labeled with AlexaFluor®488 fluorophores for characterization purposes via Confocal Microscopy. Subsequently, electrochemical deposition of photosensitizer, $[Ru(v\text{-}bpy)_3](PF6)_2$ on gold adjacent to the POEGMA for better sensitivity of the device was characterized by Square Wave Voltammetry. As the number of potential cycles increased, current also increased proving the electropolymerization of photosensitizer layer on gold. However, no further analyses were done to measure the thickness of the deposited photosensitizer layer, but based on the previous

research (Ober et al., 2014), thickness of the photosensitizer under conditions described above should approximately be around 26 nm.

Finally, ACWOP-based platform was compared to ELISA-based detection methods such direct and indirect ELISA. One of the advantages of the ACWOP-based antibody detection method is the elimination of the secondary reagent, non-specific binding, and weak signal. All these factors play an important role for possible implementation of our immunosensor in clinical diagnostics.

REFERENCES

1. Katz, Eugenii, and Itamar Willner. "Probing biomolecular interactions at conductive and semiconductive surfaces by impedance spectroscopy: routes to impedimetric immunosensors, DNA‐sensors, and enzyme biosensors."Electroanalysis 15.11 (2003): 913-947.
2. Ghindilis, Andrey L., et al. "Immunosensors: electrochemical sensing and other engineering approaches." Biosensors and Bioelectronics 13.1 (1998): 113-131.
3. Dols, Michael Walters. The Black Death in the Middle East. Princeton University Press, Guildford, Surrey., 1977.
4. Ziegler, Philip. The black death. Faber & Faber, 2013.
5. Kelly, John. "The great mortality: An intimate history of the Black Death." (2006).
6. Gottfried, Robert S. Black death. Simon and Schuster, 2010.
7. Trilla, Antoni, Guillem Trilla, and Carolyn Daer. "The 1918 “Spanish flu” in Spain." Clinical infectious diseases 47.5 (2008): 668-673.
8. Reid, Ann H., Jeffery K. Taubenberger, and Thomas G. Fanning. "The 1918 Spanish influenza: integrating history and biology." Microbes and infection 3.1 (2001): 81-87.
9. Trad, Mohamad-Ali, Dale Andrew Fisher, and Paul Anantharajah Tambyah. "Ebola in west Africa." The Lancet infectious diseases 14.11 (2014): 1045.
10. Pandey, Abhishek, et al. "Strategies for containing Ebola in west Africa."Science 346.6212 (2014): 991-995.
11. Janeway, Charles A. "How the immune system works to protect the host from infection: a personal view." Proceedings of the National Academy of Sciences98.13 (2001): 7461-7468.

12. Sompayrac, Lauren M. How the immune system works. John Wiley & Sons, 2015.

13. Janeway, Charles A., et al. Immunobiology: the immune system in health and disease. Vol. 1. Current Biology, 1997.

14. Kau, Andrew L., et al. "Human nutrition, the gut microbiome and the immune system." Nature 474.7351 (2011): 327-336.

15. Pier, Gerald Bryan, Jeffrey B. Lyczak, and Lee M. Wetzler. Immunology, infection, and immunity. ASM press, 2004.

16. Nerome, Kuniaki, et al. "Influenza vaccine." U.S. Patent No. 4,826,687. 2 May 1989.

17. Goodwin, Katherine, Cécile Viboud, and Lone Simonsen. "Antibody response to influenza vaccination in the elderly: a quantitative review." Vaccine 24.8 (2006): 1159-1169.

18. Welch, M. Elizabeth, et al. "Generalized platform for antibody detection using the antibody catalyzed water oxidation pathway." Journal of the American Chemical Society 136.5 (2014): 1879-1883.

19. Nieva, Jorge, et al. "Immunoglobulins can utilize riboflavin (Vitamin B2) to activate the antibody-catalyzed water oxidation pathway." Immunology letters103.1 (2006): 33-38.

20. Abruña, H. Denisevich, et al. "Rectifying interfaces using two-layer films of electrochemically polymerized vinylpyridine and vinylbipyridine complexes of ruthenium and iron on electrodes." Journal of the American Chemical Society103.1 (1981): 1-5.

21. Vancea, Johann, et al. "Substrate effects on the surface topography of evaporated gold films—a scanning tunnelling microscopy investigation."Surface science 218.1 (1989): 108-126.

22. Cheng, Kezia. "Electron Radiation as an Indicator of Gold Nodule Defect during E-Beam Evaporation." 2011 CS MANTECH Conference.

23. Harder, P., et al. "Molecular conformation in oligo (ethylene glycol)-terminated self-assembled monolayers on gold and silver surfaces determines their ability to resist protein adsorption." The Journal of Physical Chemistry B102.2 (1998): 426-436.

24. Herrwerth, Sascha, et al. "Factors that determine the protein resistance of oligoether self-assembled monolayers-Internal hydrophilicity, terminal hydrophilicity, and lateral packing density." Journal of the American Chemical Society 125.31 (2003): 9359-9366.

25. Senaratne, Wageesha, et al. "Dinitrophenyl ligand substrates and their application to immunosensors." Biosensors and Bioelectronics 22.1 (2006): 63-70.

26. Denisevich, P., et al. "Electropolymerization of vinylpyridine and vinylbipyridine complexes of iron and ruthenium: homopolymers, copolymers, reactive polymers." Inorganic Chemistry 21.6 (1982): 2153-2161.

27. Yang, John, Milan Sykora, and Thomas J. Meyer. "Electropolymerization of vinylbipyridine complexes of ruthenium (II) and osmium (II) in SiO2 sol-gel films." Inorganic chemistry 44.10 (2005): 3396-3404.

28. Mishin, Vladimir, et al. "Application of the Amplex red/horseradish peroxidase assay to measure hydrogen peroxide generation by recombinant microsomal enzymes." Free Radical Biology and Medicine 48.11 (2010): 1485-1491.

29. Reszka, Krzysztof J., et al. "Effects of peroxidase substrates on the Amplex red/peroxidase assay: antioxidant properties of anthracyclines." Analytical biochemistry 342.2 (2005): 327-337.

30. Haick, Hossam, et al. "Contacting organic molecules by metal evaporation."Physical

Chemistry Chemical Physics 6.19 (2004): 4538-4541.

31. Kishimoto, Tadamitsu, et al. "Regulation of Antibody Response in Different Immunoglobulin Classes I. Selective Suppression of anti-DNP IgE Antibody Response by Preadministration of DNP-Coupled Mycobacterium." The Journal of Immunology 117.2 (1976): 396-404.

32. Blonder, R., Ben-Dov, I., Dagan, A., Willner, I., Zisman, E., 1997a. Photochemically-activated electrodes: application in design of reversible immunosensors and antibody patterned interfaces. Biosens. Bioelectron. 12, 627–644.

33. Patolsky, F., Filanovsky, B., Katz, E., Willner, I., 1998. Photoswitchable antigen–antibody interactions studied by impedance spectroscopy. J. Phys. Chem. B 102, 10359–10367.

CHAPTER 2

The fabrication of microfluidic master mold by photolithography and replication of microchannels made from polydimethylsiloxane block for lab-on-a-chip applications.

Abstract

Integration of one or multiple analyses onto a single chip could be achieved via microfluidics. Microfluidic technologies consisting of channels at the micro-scale can be used in handling of samples in quantities ranging from micro- to picoliters. Fundamental goal of microfluidics is to provide reliable, cost-effective, and rapid diagnosis that could be operated by a non-technical end user, especially in isolated places lacking sophisticated facilities and well-trained personnel.

This chapter focuses on the master mold fabrication using different SU-8 permanent epoxy negative photoresist using photolithography and replication of microchannels using polydimethylsiloxane (PDMS) as a base polymer. Finally, a PDMS replica was attached on top of the platform by non-plasma methods such as solvent evaporation to preserve specific surface chemistry for antibody detection and the maximum backpressure of 10 psi was estimated using Poiseuille flow.

Introduction

Microfluidics are important devices that control and manipulate fluid flows with volume sizes ranging from microliters to picoliters. These devices received enormous attention in the fields of biology and biotechnology for the recent development of sensing devices that manipulate, analyze, and detect small quantities and operate at smaller volumes (usually on the order of 1 microliter). Microfluidics offer numerous advantages such as ability to work with small quantities, potential for cheap and portable immunosensor device fabrication, manipulation of multiple samples at once, and applicability for patient treatments in isolated areas with no laboratory settings, facilities, and well-trained technicians[34-35].

Microfluidics can also be used as point-of-care systems for diagnostics that provide real clinical value and help identify and treat serious illnesses such as diabetes or cancer. These lab-on-a-chip (LOC) devices demonstrated reliable diagnostic results and practical application to replace some laboratory tests. For example, the blood glucose test, which serves as a great example for high-impact point-of-care diagnostic devices that is being used by millions of people with diabetes. The blood glucometer is a powerful example of an immunosensing device that helps patients all over the world to monitor their glucose level and manage diabetes. For the last two decades, many research groups have been trying to build portable and fully integrated LOC devices that can be brought into a market with a clear mission to replace expensive, tedious, and complicated laboratory tests. LOC devices can make diagnostics faster, cheaper and more accessible to people in remote settings[36-40].

In this chapter, microfluidics channels were fabricated using SU-8 type epoxy based negative photoresists using photolithography to create a master mold with different shapes and sizes of lithography to make a replica of microchannels using polydimethylsiloxane (PDMS).

Challenges associated with SU-8 master mold fabrication such as edge bead removal, thermal mismatch, t-topping, overexposure, and underexposure are thoroughly discussed. These channels were attached to the platform (CHAPTER 1) by non-conventional solvent evaporation method to preserve surface chemistry and the integrated idea of the ACWOP process. Backpressure of the final device was estimated using tubing, dispensing needles, and microfluidic probe station to be around 10 psi before whole structure of the device collapses and leakages take place[41-48].

EXPERIMENTAL SECTION

The fabrication of microfluidic master mold using SU-8 type permanent epoxy negative photoresists

Silicon wafers were cleaned using Hamatech Hot Piranha (sulfuric acid and hydrogen peroxide) wafer processor and dehydrated inside oven at 200^0C for overnight or at least for 2 hours. SU-8 photoresists were applied as centered pool of fluid and spin coated to coat the substrate evenly using recommended spin and acceleration speeds depending on the desired thickness of the master mold. Then, wafers were soft-baked on a leveled hot plate at 65 ^{0}C and 95 ^{0}C depending on the SU-8 photoresist type to remove excess of the solvent and harden the photoresist followed by exposure using ABM contact aligner under a patterned photomask. Exposure times mainly depend on the thickness, uniformity of the resist and the power of the lamp. Post-exposure bake was then applied at 65 ^{0}C and 95 ^{0}C depending on the SU-8 photoresist type to complete the photoreaction initiated during the exposure and crosslink the exposed features of the film. Subsequently, wafers were developed, spray-washed with isopropyl alcohol (IPA) and dried gently with nitrogen gun. Processing guidelines for master mold fabrication utilizing different types of SU-8 resists are outlined in Table II[49-50].

TABLE II. Master mold fabrication guideline for various SU-8 negative photoresists.

SU-8 type	Spin speed	SB times (minutes)	Exposure Energy (mJ/cm^2)	PEB times (minutes)	Development (minutes)
2015 (*20 µm)	1) 500rpm for 10 s 2) 2000rpm for 30 s	5 at 95^{0}C	150-160	6 at 95 ^{0}C	20
2025 (*40 µm)	Same as for SU-8 2015	3 at 65^{0}C 6 at 95^{0}C	150-160	1 at 65 ^{0}C 6 at 95 ^{0}C	~30
2035 (*60 µm)	Same as for SU-8 2015	3 at 65 ^{0}C 9 at 95 ^{0}C	150-215	2 at 65 ^{0}C 7 at 95 ^{0}C	~30
2050 (*80 µm)	Same as for SU-8 2015	5 at 65^{0}C 10 at 95^{0}C	215	2 at 65 ^{0}C 7 at 95 ^{0}C	~30
2075 (*110 µm)	Same as for SU-8 2015	5 at 65^{0}C 20 at 95^{0}C	240	5 at 65 ^{0}C 10 at 95 ^{0}C	~30
2100 (*140 µm)	Same as for SU-8 2015	5 at 65^{0}C 25 at 95^{0}C	240-260	5 at 65 ^{0}C 12 at 95 ^{0}C	>30

*Theoretical values from spin speed vs. thickness curve recommended by MicroChem™

Preparation of PDMS and replication of master mold patterns on its surface

Polydimethylsiloxane is silicon-based organic polymer. PDMS is optically clear, biocompatible, non-toxic, flexible, non-flammable, generally inert, cheap, and easy-to-mold elastomer whose unique properties are widely in microfluidic medical devices.

Sylgard 184 pre-polymer base and Sylgard 184 curing agent (10:1 weight ratio) were mixed vigorously and stirred at least for 2-3 minutes in the plastic cup to get homogeneous white mixture filled with bubbles. The mixture was degassed using a vacuum chamber for 20 minutes or until all bubbles are gone. Alternately, the mixture could also be placed in the -20^0C freezer overnight for the same effect.

A wafer with master mold features was placed in the petri dish and the PDMS was slowly poured over wafer until covered completely (PDMS layer ~ 2mm thick). Petri dish with master mold and PDMS layer on top was placed in 60^0C oven for 60-120 minutes and cured. Then, PDMS was cut around the master mold features and peeled away from the master to get an embossed microstructure[51-52].

Sealing of PDMS stamp onto fused silica substrate and maximum backpressure estimation via microfluidic probe station

Conventional methods include oxygen plasma, indirect corona, or oxygen-rich butane gas flame. However, harsh conditions of oxygen plasma can change the surface chemistry of the platform, and essentially any organic molecules that are crucial for our immunosensor device. Therefore, two different methods were used to attach PDMS onto glass: thermal bonding and solvent evaporation. In thermal bonding, PDMS stamp was placed on top of the platform and baked in the oven at 60^0C for at least 2 hours, this is a reversible process and PDMS could be

peeled off from the glass without leaving any residues. In solvent evaporation, few ethanol drops were placed in between the platform and PDMS replica and device was left in a dry place for 24 hours to ensure ethanol was completely evaporated to seal PDMS to glass[53-56].

For backpressure estimation and leakage-free fluid flow inside microchannels, tubing and blunt dispensing needles were added to the device. A PDMS puncher was used to make clean holes in the outlet/inlet area of the device to enable tubing to chip connection and syringe pumps were used to ensure that volumetric flow rates were controlled so that pressure difference at the ends of channels could be estimated before whole system collapses[57-59].

RESULTS AND DISCUSSION

Microfluidic channels were fabricated using epoxy based SU-8 type negative photoresist by master mold fabrication using photolithography. In order to get crack-free, chemically and thermally stable master mold various pre-cautions should be taken into account.

First, for spin coating very viscous and thick SU-8 layers (> 50 μm) the film develops an edge that is thicker than the middle part of the film called the edge bead effect. Edge bead effect, is even more serious for thicker films or substrates with irregular shape and topography. Edge bead effect usually causes the poor vacuum between the photomask and the wafer due to the air gap. In such case, poor vacuum often results in poor lithography step and underexposure of the features of the master mold, causing loss of resolution, poor adhesion of the SU-8 features to the substrate and even their partial of complete detachment from the surface of the substrate. On of the possible solutions to this issue is to remove the edge bead by hand using acetone as a solvent. Another method is to remove edge bead with γ-butyrolactone (GBL) or fill the air gap with

organic solvent with precautions to avoid diffusion of the solvent into the SU-8 layer that may result in a weak structure[60-61].

Second, the soft baking process is very important in dealing with SU-8 for fabrication of the master mold for microfluidic channels. It was shown before, that soft baking and post-exposure baking conditions are very critical for thick SU-8 features. For example longer soft baking times often results in higher crack density on the top surface of the SU-8 features. These cracks are not critical for microfluidics as long as those cracks do not propagate all the way through the features and even less critical for thicker SU-8 films. These cracks usually form at the vertices of the channels and sometimes can be re-flown using hard baking at 200 ^{0}C for 4 hours at slower heating and cooling rates. The reason for internal stress and cracking induced by fast cooling or heating rates is due to the thermal mismatch between the substrate and the SU-8. It was also reported that soft baking temperatures could be reduced to lower than recommended temperatures of 95 ^{0}C to reduce the amount of cracks, however this will result in longer times, depending on the SU-8 type. Additionally, the difference of the thermal expansion coefficient between the substrate and the SU-8 (52 C^{-1}) results in the distortion of the SU-8 features and the overall geometry. In order to reduce issues resulting from distortion and internal stress, sudden temperature changes must be avoided. Therefore, gradual bake was started at the room temperature slowly reaching 65 ^{o}C, and then [if needed] to 95 ^{o}C, and finally cooling down to room temperature again at the rate of roughly 2 ^{o}C/minute. In this case, thermal stress, cracking, and detachment due to a difference in the thermal coefficient of expansion between the glass and the SU-8 layer could be greatly reduced. Over baking the wafer also results in the increased cracking density and the brittleness after the development process. On the other hand, under

baking results in too much solvent remained and the wafer will stick to the photomask. This often results in the SU-8 features that may melt off or detach during the development[62-65].

Third, to prevent the top of the SU-8 layer from flowing over and wrinkling after spin coating SU-8, the substrate was covered with a glass dish leaving a small gap for vapors to dry and escape slowly [for thick SU-8 layers].

Finally, when exposing wafers, wavelengths shorter than 365 nm were filtered out to prevent T-topping phenomenon, where the top part of the resist film is over exposed comparing to the bottom part resulting in negative sidewall profile. The reason lies in the fact that SU-8 is optimized for near ultra violet exposure (near UV, 350-400 nm) and has high actinic absorption below 350 nm. In the previous research work, T-topping effect of the SU-8 features was eliminated using high-wavelength pass optical filter to isolate wavelengths below 300 nm during the exposure to get high aspect-ratio structures of (700 micron tall) cilium made of SU-8 epoxy and silicon piezoresistive strain sensors[66-68].

It's important to note that spin coating, soft baking, exposure, post baking, and development processes should be optimized for different SU-8 structures depending on the thickness, application, aspect-ratio, resist type, and supporting substrate. Recommended development rates will also change with different aspect ratios and thickness as well as the amount of sonication, agitation, and the temperature.

Preparation of PDMS replica and its binding to the platform

Preparation of the PDMS and replication of master mold patterns on its surface is done via widely known and relatively simple soft lithography process. PDMS was prepared using polymer base and curing agent, then poured over SU-8 master mold structure and cured in the oven at 60 ^{0}C for at least 2 hours. Finally, PDMS replica with microchannels was peeled away

from the substrate to get embossed microstructure. Polydimethylsiloxane (PDMS) was chosen due to its chemical and physical properties that suit our immunosensor design. PDMS is a non-toxic, cheap and easy-to-mold elastomer making it a strong candidate for integration in portable and inexpensive immunosensor device[69].

Sealing of the PDMS to the surface of the platform was achieved by evaporation of the ethanol between the surfaces of the platform and PDMS replica. This method is non-destructive compared to other conventional methods such as oxygen plasma or corona discharge. Methods that use harsh conditions of oxygen plasma tend to make strong (covalent) bonding between the glass and the PDMS. However, these methods also change and sometimes destroy crucial surface chemistry of the platform, which is needed for successful implementation of the fundamental idea of the ACWOP process.

Backpressure estimation based on Poiseuille flow via microfluidic probe station

Quantitative measurements of the strength of adhesion of microfluidics to the platform was estimated via microfluidic probe station based on Poiseuille flow, where fluid is driven though a straight channel by applying pressure difference at both ends, Δp. The gravity inside channel is balanced by hydrostatic pressure, and fluid motion is primarily in the x-direction. Therefore, based on a maximum flow rate before device collapses, maximum backpressure could be estimated using equation 1:

(1) $$\boldsymbol{Q = \int dydz v_x(y,z) = A v_{avr}}$$

where Q is the volumetric flow rate, $\boldsymbol{v_{avr}}$ is the average velocity and $\boldsymbol{A}$ is the cross-section area. Furthermore, this equation can be simplified for rectangular shaped channels assuming that height of the channels, h, are smaller than the width, w, of the channels in length (Eq.1.1):

(1.1) $$\boldsymbol{Q \approx \left[1 - 0.630 \frac{h}{w}\right] \frac{h^3 w}{12 \eta L} \Delta p}$$

where, h is the height of the channels, w is the width of the channels, L is the length of the channels, and Δp is the pressure difference. It's important to note that even for the case where h = w, the error of the result from Equation 1.1 is 13 % and for the case where h = w/2 is 0.2% (H. Bruus, 2011). Based on the geometry of the channels (h = 180 microns, w = 400 microns, L = 21.5 mm) used to quantify the strength of our immunosensor device and measured flow rate (~27 ml/min) via microfluidic probe station, maximum backpressure was estimated to be 10 psi. Beyond this pressure, leakages start to take place inside the microfluidic immunosensor system. There are no literature values of backpressure estimation for microfluidic channels using the solvent evaporation attachment process of PDMS replica to the solid substrate.

CHARACTERIZATION OF THE SU-8 MASTER MOLD STRUCTURES AND MICROFLUIDIC DEVICE

All wafers were inspected under the microscope for defects, excessive cracking, adhesion failures, and characterized by profilometry to measure film thickness. Surface characterization of the platform by contact profilometer with 1mm scan length confirmed the step height, width, and wall-to-wall distance of the SU-8 structures (see Fig.10-11).

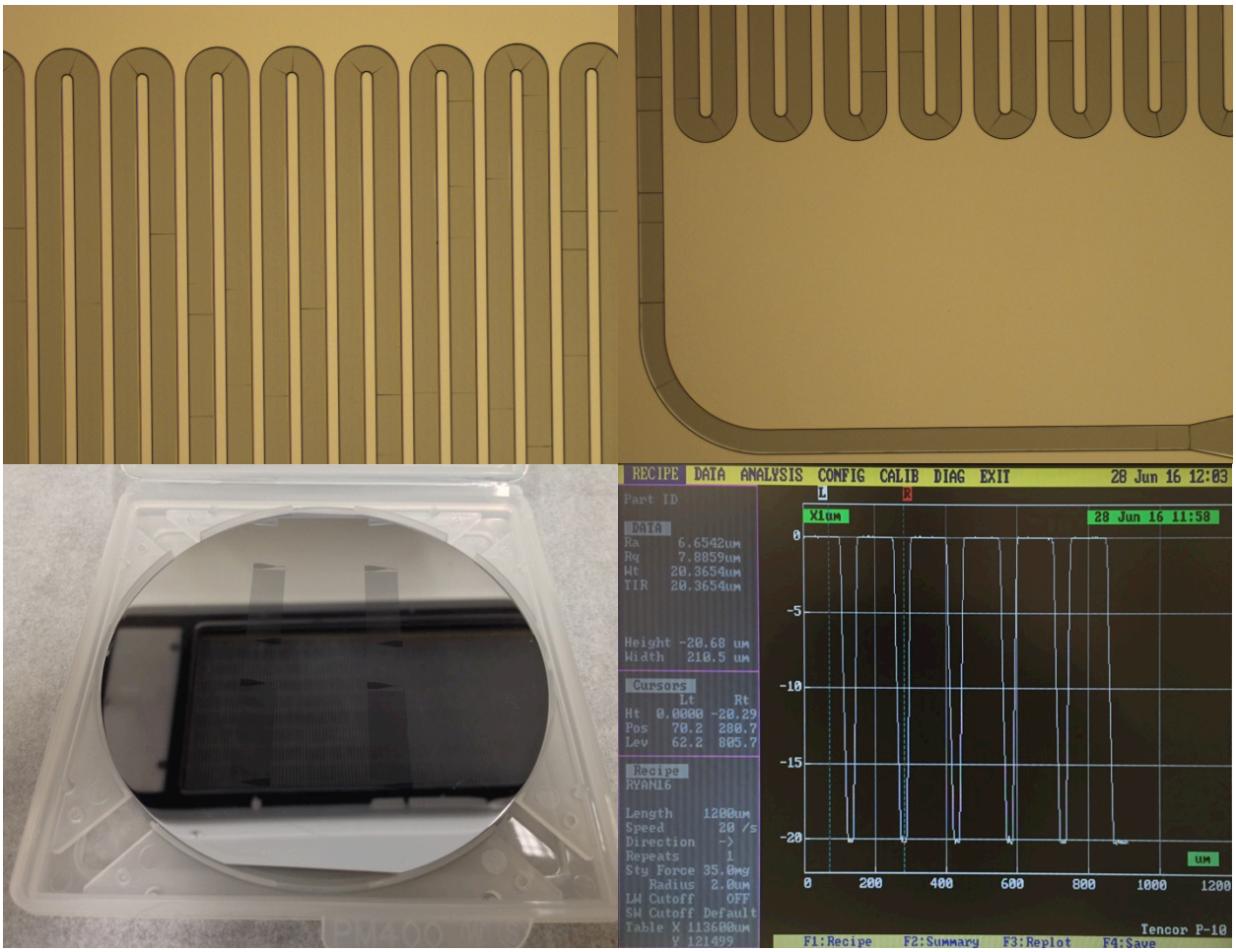

Figure 10. Illustration of patterned master mold made of SU-8 2015 with channel width = 100 μm, thickness = 20 μm, and wall-to-wall distance = 50 μm measured by Profilometer.

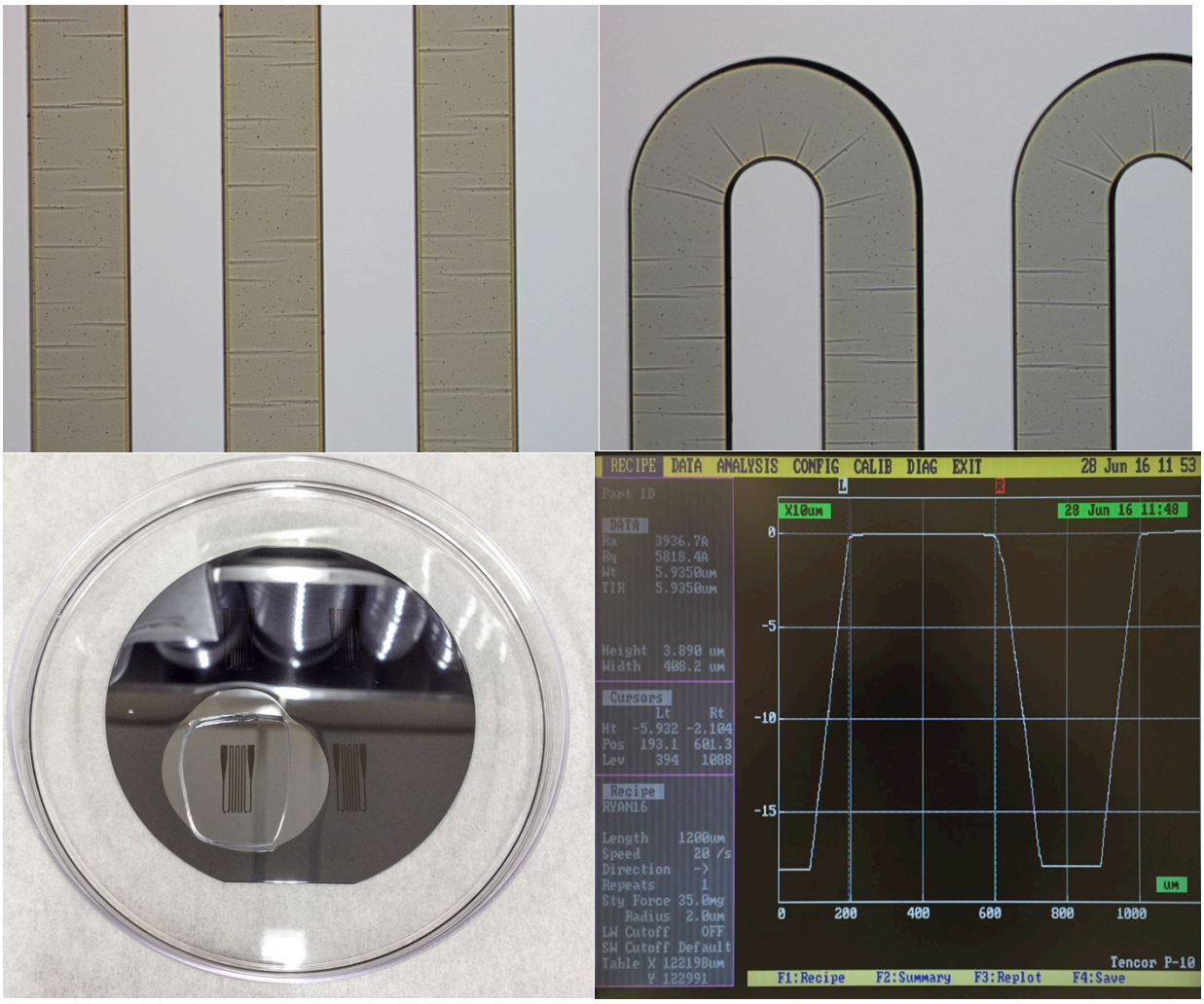

Figure 11. Illustration of patterned master mold made of SU-8 2100 with channel width = 400 μm, thickness = 180 μm, and wall-to-wall distance = 400 μm measured by Profilometer and covered with polydimethylsiloxane layer (1-2 mm thick) on top.

Final device characterization was performed using microfluidic probe station with constant volumetric flow rate to check the microfluidic immunosensor device for leakages (Fig.12). Maximum flow rate before leakages take places was approximately 27 ml/min for PBS solution (fluid viscosity = 1.05 cP, and fluid density 1 g/cm^3), which results in the maximum backpressure estimation described above of 10 psi. These results also could be used for determining the Reynolds number, and consequently the fluid flow type (laminar, transitional, turbulent) based on the velocity, flow rate, and the geometry of the channels if needed.

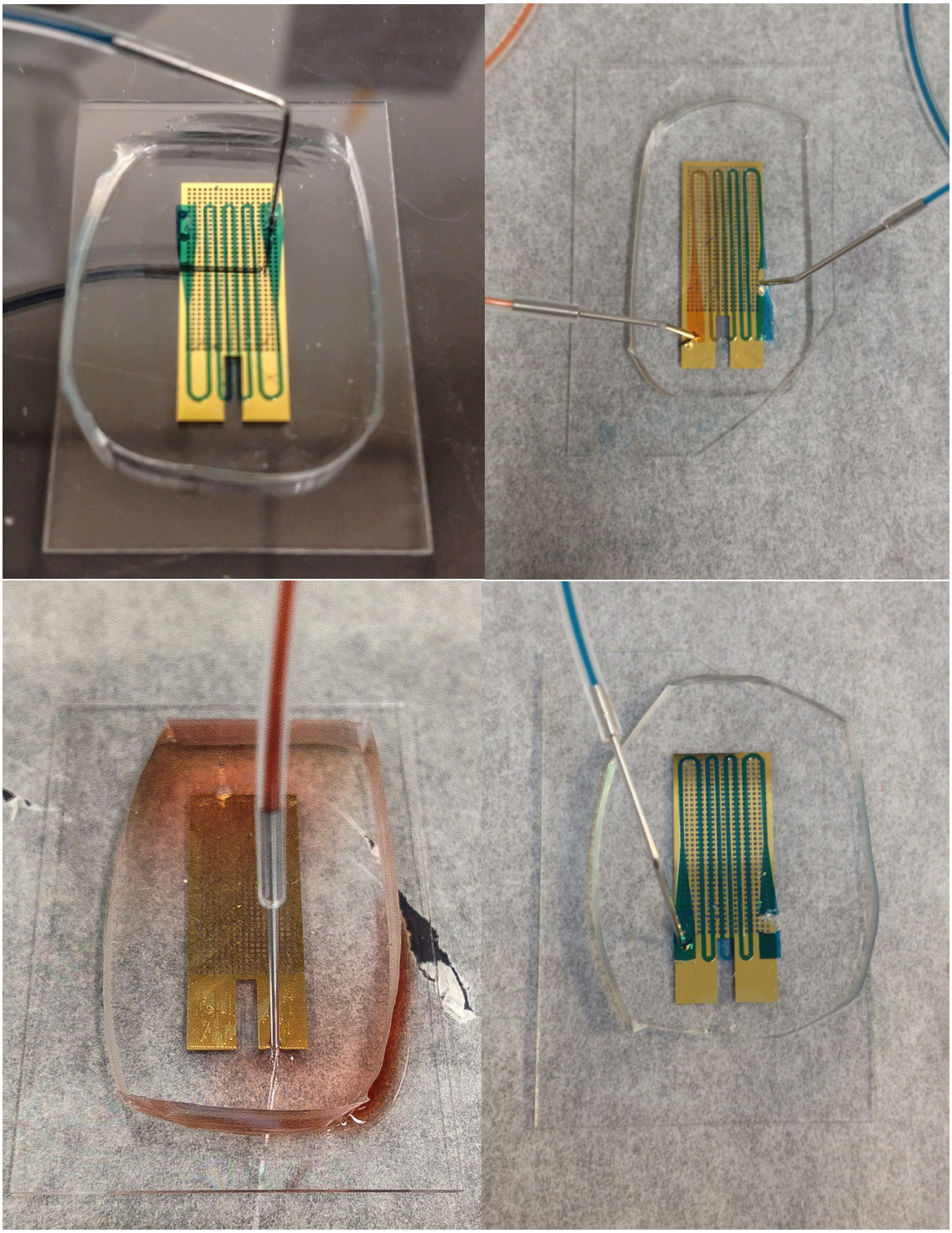

Figure 12: Three versions of microfluidic immunosensor device. Different master molds with 180-µm thick channels (1) and (1.1), 20-µm thick channels (2) and 80-µm thick (3) channels. Two color dyes (green, red) were used to show proper fluid flow inside the PDMS channels with no leakage (red dye), leakage (red dye).

Conclusion

In this chapter, different master molds were successfully fabricated using SU-8 negative epoxy based photoresist via optical lithography. Depending on the application, thicker or thinner layers could be manufactured depending on the SU-8 type. Challenges associated with thermal mismatch, detachment, overexposure, underexposure, edge bead effect, cracking density and negative sidewalls profile could be minimized by optimizing soft-baking and post-baking temperatures, exposing times, cooling and heating rates. Then, PDMS microchannels were manufactured by soft lithography technique and attached to the platform by solvent evaporation (ethanol) method. Ethanol evaporation creates a non-covalent (weak) and reversible attachment of the PDMS to the platform. One of the advantages of using solvent evaporation method lies in its non-destructive nature to the surface of the platform, which is essential in integration ACWOP-based antibody detection method in our immunosensor device. Finally, the fluid flow was characterized and quantified via microfluidic probe station, i.e. maximum backpressure of 10 psi was calculated based on the Poiseuille flow.

REFERENCES

34. Whitesides, George M. "The origins and the future of microfluidics." Nature442.7101 (2006): 368-373.

35. Stone, Howard A., Abraham D. Stroock, and Armand Ajdari. "Engineering flows in small devices: microfluidics toward a lab-on-a-chip." Annu. Rev. Fluid Mech. 36 (2004): 381-411.

36. Chin, Curtis D., Vincent Linder, and Samuel K. Sia. "Commercialization of microfluidic point-of-care diagnostic devices." Lab on a Chip 12.12 (2012): 2118-2134.

37. Tüdős, Anna J., Geert AJ Besselink, and Richard BM Schasfoort. "Trends in miniaturized total analysis systems for point-of-care testing in clinical chemistry." Lab on a Chip 1.2 (2001): 83-95.

38. Myers, Frank B., and Luke P. Lee. "Innovations in optical microfluidic technologies for point-of-care diagnostics." Lab on a Chip 8.12 (2008): 2015-2031.

39. Sia, Samuel K., and Larry J. Kricka. "Microfluidics and point-of-care testing."Lab on a Chip 8.12 (2008): 1982-1983.

40. Soper, Steven A., et al. "Point-of-care biosensor systems for cancer diagnostics/prognostics." Biosensors and Bioelectronics 21.10 (2006): 1932-1942.

41. Shirtcliffe, Neil J., et al. "The use of high aspect ratio photoresist (SU-8) for super-hydrophobic pattern prototyping." Journal of Micromechanics and Microengineering 14.10 (2004): 1384.

42. Lorenz, Hubert, et al. "SU-8: a low-cost negative resist for MEMS." Journal of Micromechanics and Microengineering 7.3 (1997): 121.

43. Chan-Park, Mary B., et al. "Fabrication of large SU-8 mold with high aspect ratio

microchannels by UV exposure dose reduction." Sensors and Actuators B: Chemical 101.1 (2004): 175-182.

44. Xia, Younan, and George M. Whitesides. "Soft lithography." Annual review of materials science 28.1 (1998): 153-184.

45. Anhoj, Thomas A., et al. "The effect of soft bake temperature on the polymerization of SU-8 photoresist." Journal of Micromechanics and Microengineering 16.9 (2006): 1819.

46. Xia, Younan, et al. "Replica molding using polymeric materials: A practical step toward nanomanufacturing." Advanced Materials 9.2 (1997): 147-149.

47. Duffy, David C., et al. "Rapid prototyping of microfluidic systems in poly (dimethylsiloxane)." Analytical chemistry 70.23 (1998): 4974-4984.

48. Bruus, Henrik. “Governing Equations in Microfluidics.” (2014): 1-28.

49. Keller, Stephan, et al. "Processing of thin SU-8 films." Journal of micromechanics and microengineering 18.12 (2008): 125020.

50. Chan-Park, Mary B., et al. "Fabrication of large SU-8 mold with high aspect ratio microchannels by UV exposure dose reduction." Sensors and Actuators B: Chemical 101.1 (2004): 175-182.

51. Sia, Samuel K., and George M. Whitesides. "Microfluidic devices fabricated in poly (dimethylsiloxane) for biological studies." Electrophoresis 24.21 (2003): 3563-3576.

52. McDonald, J. Cooper, and George M. Whitesides. "Poly (dimethylsiloxane) as a material for fabricating microfluidic devices." Accounts of chemical research35.7 (2002): 491-499.

53. Makamba, Honest, et al. "Surface modification of poly (dimethylsiloxane) microchannels." Electrophoresis 24.21 (2003): 3607-3619.

54. Aran, Kiana, et al. "Irreversible, direct bonding of nanoporous polymer membranes to PDMS or glass microdevices." Lab on a Chip 10.5 (2010): 548-552.

55. Eddings, Mark A., Michael A. Johnson, and Bruce K. Gale. "Determining the optimal PDMS–PDMS bonding technique for microfluidic devices." Journal of Micromechanics and Microengineering 18.6 (2008): 067001.

56. Bhattacharya, Shantanu, et al. "Studies on surface wettability of poly (dimethyl) siloxane (PDMS) and glass under oxygen-plasma treatment and correlation with bond strength." Journal of microelectromechanical systems14.3 (2005): 590-597.

57. Haubert, Kathryn, Tracy Drier, and David Beebe. "PDMS bonding by means of a portable, low-cost corona system." Lab on a Chip 6.12 (2006): 1548-1549.

58. Harris, Joseph, et al. "Non-plasma bonding of PDMS for inexpensive fabrication of microfluidic devices." JoVE (Journal of Visualized Experiments)9 (2007): e410-e410.

59. Reymond, Frédéric, Joël S. Rossier, and Hubert H. Girault. "Polymer microchips bonded by O2-plasma activation." Electrophoresis 23 (2002): 782-90.

60. Mata, Alvaro, Aaron J. Fleischman, and Shuvo Roy. "Fabrication of multi-layer SU-8 microstructures." Journal of micromechanics and microengineering 16.2 (2006): 276.

61. Tseng F G, Chuang Y J and Lin W K 2001 Reduction of diffraction effect of UV exposure on Su-8 negative thick PR by air gap elimination Proc. HARMST 4th Workshop on High Aspect Ratio Micro-structure Technology (Baden-Baden, Germany) pp 73–4

62. Zhang J, Tan K L and Gong H Q 2001 Characterization of the polymerization of SU-8 PR and its applications in micro-electro-mechanical systems (MEMS) Polym. Test. 20 693–701

63. Bogdanov A L and Peredkov S S 2000 Use of SU-8 PR for very high aspect ratio x-ray lithography Microelectron. Eng. 53 493–6

64. Eyre B, Blosiu J and Wiberg D 1998 Taguchi optimization for the processing of EPON SU-8 resist Proc. MEMS'98 (IEEE, Heidelberg, Germany) pp 218–22

65. Lorenz H, Laudon M and Renaud P 1998 Mechanical characterization of a new high-aspect-ratio near UV-PR Microelectron. Eng. 41-42 371–4

66. Lin, Che-Hsin, et al. "A new fabrication process for ultra-thick microfluidic microstructures utilizing SU-8 photoresist." Journal of Micromechanics and Microengineering 12.5 (2002): 590.

67. Shirtcliffe, Neil J., et al. "The use of high aspect ratio photoresist (SU-8) for super-hydrophobic pattern prototyping." Journal of Micromechanics and Microengineering 14.10 (2004): 1384.

68. Chen, Nannan, et al. "Development and characterization of high sensitivity bioinspired artificial haircell sensor." Proceedings of Solid-State Sensors, Actuators, and Microsystems Workshop. Vol. 6. 2006.

69. Brittain, Scott, et al. "Soft lithography and microfabrication." Physics World11.5 (1998): 31.

CHAPTER 3

Specific detection of fluorescently labeled (AlexaFluor®488) anti-DNP IgE antibodies using dinitrophenyl ligands as haptens via microfluidics and future directions in fabricating more sophisticated microfluidic immunosensor devices for antibody detection.

Abstract

Specific detection of antibodies can be achieved by chemically modifying the surface with oligo(ethylene glycol) moieties and hapten groups that control specific and non-specific binding of appropriate antibody-antigen complexes. As a model system, poly(oligo ethylene glycol methacrylate) [POEGMA] was polymerized on fused silica glass substrate using atom-transfer radical polymerization (ATRP) and functionalized with 2,4-dinitrophenyl (DNP) ligands as hapten groups that attach specifically to anti-DNP IgE antibodies. Oligo(ethylene glycol) moieties intend to align the functional group away from the surface and make them available to the anti-DNP IgE antibodies that were labeled with AlexaFluor®488 for fluorescent detection. Mean gray value (also known as mean fluorescence or average intensity) and background fluorescence were measured for two different concentrations of fluorescently labeled anti-DNP IgE antibodies that were incubated on the surface of the platform via injection through microfluidic channels. Finally, future directions in fabricating more sophisticated microfluidic immunosensor device such as performing multiple analyses, controlling fluid flow, separating different analytes, and increasing the throughput of the device.

Introduction

Immunosensors are analytical devices based on specific recognition of the analyte (antigens) by antibodies to form a stable system. This system's operation depends on the interaction between antigen or the analyte and the specific binding agent such as antibodies and belongs to a class of detection also known as the immunoassay. Immunoassay is a rapid test for specific detection of molecules, usually antibodies that attach specifically to the analyte such as an antigen. The whole process can be used in clinical sciences for patient monitoring, disease diagnostics, and vaccine development[70-71]. For example, Dr. Navarro has developed a HCG urine immunoassay for detecting all types of cancer. His simple test gave 31 positive results for 32 patients that were proven to have a cancer. This test was able to detect a brain cancer, skin cancer, cancer of the bones, and others well in advance (up to two years) of the initial signs for the disease to appear. It also can be used in biological research, for studying certain molecules, tracking proteins or analyzing certain hormones because of their specificity and sensitivity. In addition, it is widely used in industries such as the food industry for monitoring purity of water and quality control in food processing assessment. In the pharmaceutical industry, these principles are used for detection of toxins and studying the effects of certain drugs[72].

The development of immunoassay technology is still an active area of research in the field of clinical diagnosis. Immunosensors usually operate with small volumes, typically less than 1 microliter, making these devices to be the best candidates for future integration in isolated areas with minimal resources, facilities, and trained personnel. Further development of the complexity, functionality, and automation of the immunosensor devices will improve patient monitoring and the ability to perform multiple tests for several diseases in a single run. Immunosensor technology needs further development in its specificity, sensitivity as well as

throughput to fully replace conventional, often more complicated, but also more reliable laboratory-testing methods.[73-74]

There are different types of immunosensors based on detection methods such as electrochemical, optical, thermometric, and others. In addition, for example electrochemical sensors can be further divided into smaller sub-parts such as potentiometric, trans-membrane potential, electrode potential, field-effect transistor, amperometric, conductometric, and so on. However, in this chapter only an optical sensor will be discussed. As was mentioned before even optical immunosensors can be subdivided into smaller groups based on detection methods. For example, detection based on changes in adsorption, fluorescence, luminescence, light scattering, refractive index, etc.[75-76]

In our immunosensor, fluorescence based detection of anti-DNP IgE antibodies labeled with AlexaFluor®488 through the use of 2,4-dinitrophenyl modified POEGMA brushes was studied. It was shown before, that IgE antibodies bind to the DNP groups using monovalent and bivalent attachment. Through the use of microfluidics fabricated in chapter 2 using simple photolithography and a soft-lithography process and the surface modified platform manufactured in chapter 1 by the lift off process, antibodies were incubated. Incubation of fluorescently labeled anti-DNP IgE antibodies was performed by rinsing the surface of the platform with buffer solution, followed with BSA for blocking non-specific attachment of the antibodies to the parts of the device and the PDMS walls of the channels. After incubating IgE antibodies in the dark for at least 1 hour, any unbound antibodies were rinsed with buffer solution at least three times to minimize non-specific fluorescence measurements that will affect intensity measurements of the brightness. Confocal Microscopy was used to study and analyze mean, maximum and minimum gray value for the 16-bit fluorescent images. A gray value was then converted to fluorescence

intensity for the region of interest and the background. Note, that the purpose of the findings in this chapter is to confirm specific attachment of the IgE antibodies to the DNP-functionalized POEGMA brushes and comparison to the background fluorescence. It was also shown that acquisition parameters such as master gain voltage strongly affect not only the absolute intensity values of the fluorescent image but also the ratio between intensity of the region of interest and background fluorescence[77-79].

All parts of the device including platforms, microfluidic stamps, labeled antibodies were fabricated in the same batch under the same conditions and analyzed at the same time for comparison purposes.

EXPERIMENTAL SECTION

Incubation of anti-DNP IgE antibodies onto platform via microfluidic injection

Polymerization of POEGMA by atom-transfer radical polymerization and subsequent functionalization of POEGMA brushes with 2,4-dinitrophenl (DNP) groups onto fused silica substrate were carried out exactly as described in CHAPTER 1. All platforms were rinsed with phosphate-buffered saline (PBS) solution, pH 7.2, containing 10 mg/ml of bovine serum albumin (BSA) via injection through microfluidics using dispensing needles. Two different concetrations of anti-DNP IgE antibodies (10 and 25 μg/ml) labeled with AlexaFluor®488 were injected though microchannels and incubated inside the microfluidic immunosensor device in the dark for an hour at room temperature. Finally, all samples were rinsed multiple times with PBS solution (containing 1 nM ethylenediaminetetraecetic acid) to wash off any unbound antibodies.

Fluorescence detection and fluorescence intensity measurement of specifically bound anti-DNP IgE antibodies by Confocal Microscopy.

All samples were analyzed using Zeiss LSM 880 Inverted microscope at the Biotechnology Resouce Center (BRC), Institute of Biotechnology. All platforms were analyzed with the 40X magnification objective (oil immersion, numerical aperture NA = 1.4, and working distance WD = 0.13 mm) by placing samples on glass cover slips (No.1.5, size 22 x 40 mm) with thin layer of water in between and focusing from below. Suitable excitation and emission beam splitters, and appropriate mirror units were used for AlexaFluor®488 dye. Same acquisition parameters such as but not limited to laser line attenuator transmission, scanning mode and speed, gain master, bit depth were applied across all samples to get a reliable comparison and analyzed using Fiji (ImageJ, version 2.0.0-rc-48/1.51) software.

RESULTS AND DISCUSSION

Fused silica platforms were fabricated via photolithography using a double layer of positive and lift off resist. The lift-off process was used to create an isolated pattern of gold lines on a fused silica surface by Au deposition via electron gun evaporation. E-beam evaporation method of gold lines is the preferred metal deposition method for creating isolated patterns without fencing issues. Then, these platforms were polymerized with POEGMA brushes using the ATRP polymerization technique and silane initiator the thickness of POEGMA brushes was characterized and measured using tapping mode AFM. In tapping mode AFM, a blunt instrument was used to make a scratch on the fused silica surface and penetrate through POEGMA brushes to make a step profile of the surface. Platforms with POEGMA-modified surface were functionalized with DNP groups (described in chapter 1) as hapten molecules for specific

attachment of anti-DNP IgE antibodies. The specific attachment of the antibodies was previously confirmed via Confocal Microscopy.

Microfluidic channels made of PDMS were manufactured using SU-8 processing via photolithography to create a master mold pattern and soft lithography techniques were used for making a PDMS replica of the SU-8 patterns of the microchannels. PDMS replica of the SU-8 patterns was attached to the platform by ethanol evaporation techniques described in CHAPTER 2. Through the use of PDMS punch, holes were made for tubing and dispensing needles were attached for fluid delivery inside and outside the channels. Anti-DNP IgE antibodies were fluorescently labeled with AlexaFluor®488 using a standard procedure for fluorescence measurements by Confocal Microscopy. These labeled antibodies were incubated through microfluidics using microfluidic probe station under steady-state condition in order to prevent detachment of the PDMS channels. It was shown in CHAPTER 2, that the maximum backpressure of the device before the system collapses is 10 psi, alternatively the maximum volumetric flow rate is 27 ml/min. Hence, injection of antibodies was performed so that the flow rate or pressure inside channels were kept below critical values. Moreover, incubation was performed in the dark for at least one hour and analyzed by Confocal Microscopy on the same day.

It was shown previously (Ober et al., 2006) that monoclonal anti-DNP IgE antibodies attach to the DNP functional groups through monovalent and bivalent attachment and that nonspecific adsorption (for 1.0 and 0.1 μg/ml anti-DNP IgE antibodies) was determined to be up to 10 times lower than the specific adsorption of antibodies. Nonspecific attachment of antibodies (rat IgE, MW 180, 000) to the QCM crystal surface for 1 and 0,1 μg/ml was determined to be 8.8×10^{-13} mol/cm^2 and 1.3×10^{-13} mol/cm^2, respectively, with no detectable

change in frequency for the sample with 0.01 μg/ml antibody concentration. Apparent affinity and site density was also measured assuming homogeneous ligand distribution on the surface using Langmuir adsorption isotherm and fitting algorithm by Levenberg-Marquardt.

However, in our case, the presence of PDMS channels may provide sites for non-specific attachment of antibodies to the surface of the device. Therefore, all samples were rinsed with bovine serum albumin (BSA) to block nonspecific adsorption of antibodies on the walls of the PDMS channels and other surfaces of the device[80]. After incubation of antibodies, platforms were rinsed with buffer solution multiple times to minimize non-specific fluorescence from any unbound antibodies floating on the surface of the platform. PDMS stamp was detached away from the platform before fluorescence measurements. Detachment of the PDMS from the platform leaves no contamination on the surface due to the weak and reversible nature of the bond between the PDMS channels and the platform. Finally, Confocal Microscopy was used to analyze and measure the mean gray value and mean background gray value. The mean gray value and the mean background gray value can be used as a mean fluorescence and mean background fluorescence, respectively. Other parameters such as modal, minimum, maximum gray values and their standard deviations can be measured using Fiji software all at once, however these parameters are insignificant for fluorescence measurement purposes[81-82].

The sample with higher antibody concentration of 25 μg/ml was saturated at master gain of 840 V. More than 80% of the total area selected was oversaturated in intensity when analyzing using Fiji software. In order to measure the ratio of the average intensity of brightness between the region of interest and the background intensity more precisely, the master gain was lowered to 650 and 550. The master gain (MG) must be regulated for accurate brightness measurements to keep minimum intensity levels above 0 and maximum intensity levels below its

maximum value of 65536 for 16-bit image. Therefore, minimum intensity levels and maximum intensity levels were set to 1 and 65529 values, respectively. Average intensity of the brightness for the region of interest was 25,000, 10,000 and 1,700 and the background average intensity was 1000, 227, and 130 for MG of 708 V, 650 V and 550 V, respectively. Threshold area for all regions of interest exceeded 99%, meaning that less than 1% of the total area selected was saturated for gain master values of 708 V, 650 V and 550 V. It's clear that increasing gain master voltage increases the average brightness intensity by amplifying weak signal and boosting noise levels. Ratios of average intensities between region of interest and background fluorescence were on the same order of magnitude, more precisely 25, 44, and 13 for master gains of 708 V, 650 V, and 550 V, respectively. Even though, at voltage of 708 there was no saturation of pixels, but the ratio of average intensities between region of interest and background fluorescence decreased comparing to the voltage of 650. Changes in gain master voltage have little effect on the background fluorescence intensity levels comparing to the effect on fluorescence intensity levels of the region of interest. Hence, increasing gain master increases the ratio of average intensities between region of interest and background fluorescence below gain master voltage of 708 V, which is under saturation limit. Further research on the relationship between master gain voltage and intensity levels should be studied more comprehensively in order to make more reliable comparison between the ratios of average intensities between region of interest and background fluorescence at different gain master voltages.

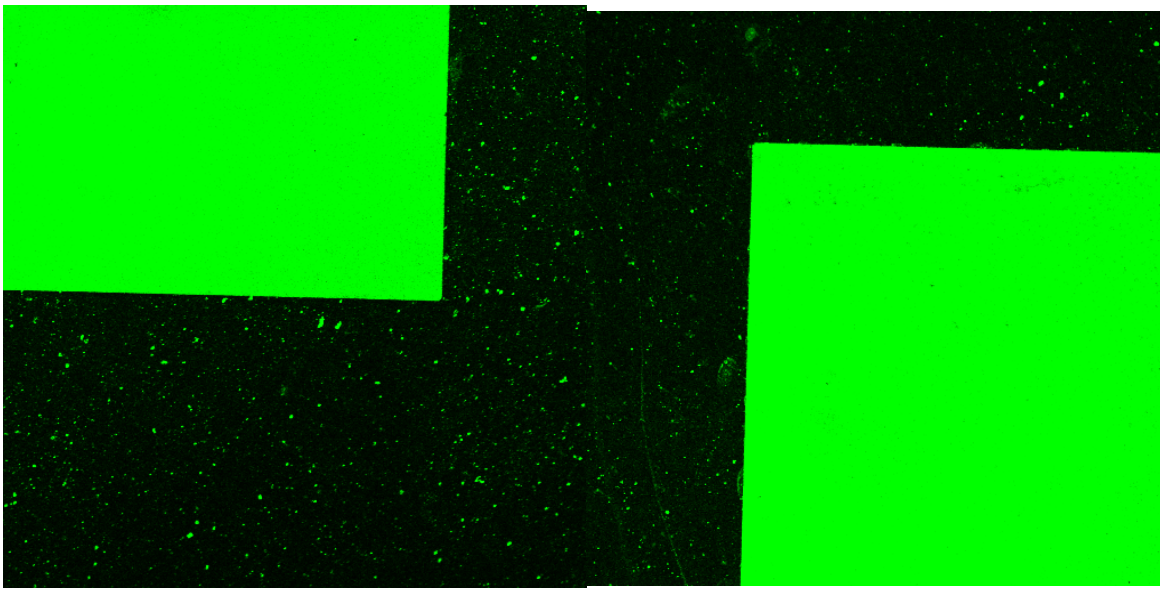

Figure 13. Fluorescence images of the saturation of the 25 μg/ml anti-DNP IgE antibodies at 840 master gain voltage

A sample with antibody concentration of 10 μg/ml was not saturated at gain master of 840 V (Fig. 14). Average intensity of the brightness for the region of interest was 11,000 and the background average intensity was 1200 for master gain of 840 V. Threshold area for region of interest again exceeded 99% at 840 V. Ratio of average intensity between region of interest and background fluorescence was 9 for master gain of 840 V, respectively.

Only ratios of the mean fluorescence and mean background fluorescence were measured. Mean intensities of the two different concentrations of IgE were not compared due to the fact that more in-depth analysis is required for accurate measurements such as taking into account different type of noises such as Poisson noise, readout noise. In addition, mean intensities of background fluorescence are also dependent on the purity of the platform (gold particles tend to fluoresce) and the point at which acquisition of the fluorescent image was made. For instance, at the point of injection mean fluorescent intensities and mean background intensities are higher from those measured away from the point of injection.

The idea of fluorescence measurements presented in this research was to confirm specific attachment of IgE to the functionalized polymer brushes that were grown on gold only. It was also shown, that the average intensities increased with master gain voltage. Mean fluorescence and background fluorescence used in this research is simply mean gray values of the point of interest and background noise, respectively.

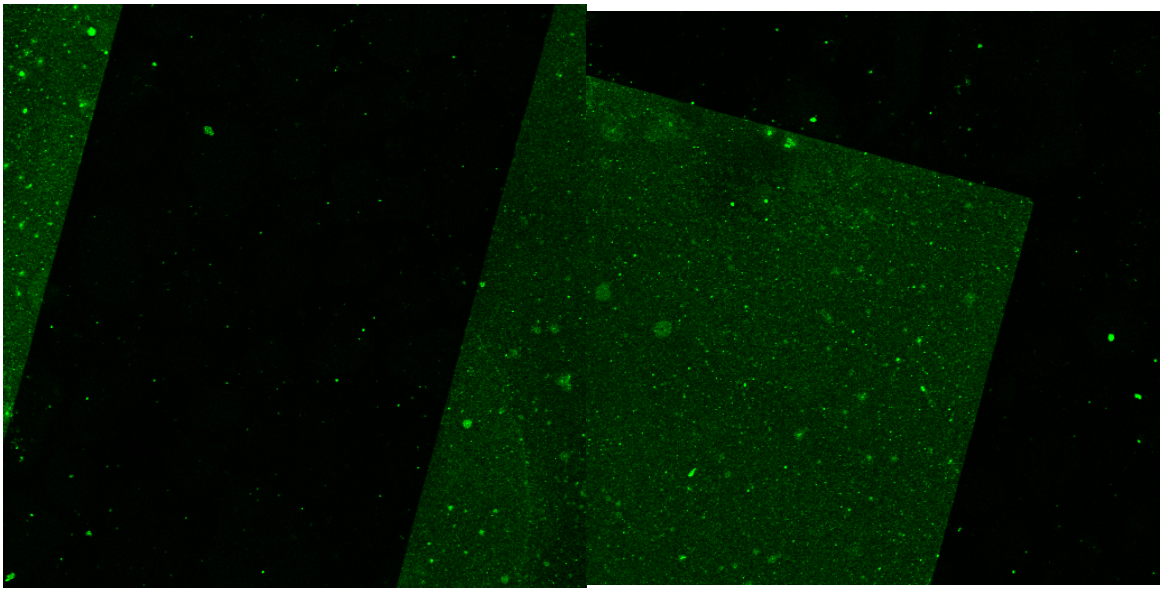

Figure 14. Fluorescence images of the platforms based on the ACWOP and specific binding of the POEGMA functionalized brushes to anti-DNP IgE antibodies at concentration of 10 μg/ml.

For more accurate results, it's essential to keep samples clean of dust and rinse multiple times with PBS (1mM EDTA) solution to wash off any unbound antibodies that may affect fluorescence measurements. In the case of unbound antibodies, the average intensity of the region of interest could be significantly higher than the actual value. One of the ways to measure average intensity more precisely is to scan different parts of the device incubated with antibodies. It was clear from the experimental results that the average intensity tends to be higher at the point of injection and decreases as you scan away from it. In addition, intensity levels should be optimized in such way so that the saturation of pixels does not take place for accurate ration measurements between the region of interest and the background fluorescence. Finally, reliable comparison all samples should be produced, functionalized, incubated in the same batch and analyzed at the same time.

Conclusions

In this chapter, two different concentrations of fluorescently labeled anti-DNP IgE antibodies were incubated via injection through microfluidics. Confocal Microscopy was used to analyze and measure average intensities for the fluorescence of the region of interest and background fluorescence and their respective ratios at different gain master voltages were calculated. Gain master voltage was optimized to keep intensity levels of the pixels above and below its minimum and maximum values, respectively for reliable results. For 16-bit image minimum and maximum intensity values were set to 1 and 65529. However, further research should be done for complete understanding of the effect of the gain master voltage on intensity values.

The sample with a higher antibody concentration of 25 μg/ml showed average intensity of the region of interest to be 25,000, 10,000 and 1,700 and the background average intensity to be 1000, 227, and 130 for GM of 708 V, 650 V and 550 V, respectively. Threshold area for all regions of interest exceeded 99%, meaning that less than 1% of the total area selected was saturated for gain master values of 840 V, 708 V, 650 V and 550 V. Ratios of average intensities between region of interest and background fluorescence were 25, 44, and 13 at master gain voltage of 708 V, 650 V, and 550 V, respectively. Increasing gain master voltage increased intensity levels, however the ratio of average intensities between region of interest and background fluorescence decreased at the gain voltage of 708 V, even though it was below saturation limit.

The sample with a lower antibody concentration of 10 μg/ml was not saturated at gain master of 840 V. Average intensity of the brightness for the region of interest was 11,000 and the background average intensity was 1200 for master gain of 840 V. Threshold area for region of interest again exceeded 99% at 840 V. Ratio of average intensity between region of interest and background fluorescence was 9 at master gain voltage of 840 V[83].

FUTURE DIRECTIONS

Microfluidic immunosensor based on the ACWOP process presented in this research can be optimized depending on the complexity of intended applications. Our device consists of a single integrated pattern with inlet/outlet system for single-sample testing. However, one of the advantages of microfluidics is the flexibility to create more sophisticated systems with mixers, valves for separation, and detectors for multi-analyte immunosensing. Adding multiple channels or designing more complex structures of the microfluidics can be optimized without significantly affecting the time for fabricating such systems. In the work done by Bromberg and Mathies, microfluidic device with 48 channels were designed for rapid electrophoretic separation to analyze fluorescein-labeled and non-labeled 2,4,6-trinitrotoluene (TNT) for anti-TNT antibody binding[84].

Instead of integrating multiple channels, Jiang and Ng (2003) fabricated a branched network of microchannels that use serial dilution for analyzing multiple antibodies quantitatively in parallel using very small sample volumes, less than 1 microliter per experiment. They incorporated a microdilutor network for diluting serum containing HIV antibodies and chaotic advective mixers (CAMs) for mixing to achieve antibody-antigen interaction, where antigens were presented in patterns over the polycarbonate membrane.

Researchers at the Zurich Research Laboratory invented micromosaic immunosensors in which 16 or more independent microchannels were integrated to detect C-reactive protein (CRP), myoglobin (Mb), and cardiac Troponin I. This system includes microfluidic network in which liquid is displaced using capillary forces and requires no external pumps or power equipment to power up the immunosensing device making it “autonomous”. Finally, it was shown that CRP

could be detected down to 30 ng/ml, which is within clinically relevant concentrations for the coronary hear disease diagnostics[85].

In another technique, Japanese researchers fabricated an immunosorbent assay integrated into a glass platform with polystyrene microbeads for creating a high surface area and thermal lens microscope as a detector for analyzing secretory human immunoglobulin A (s-IgA). Integrating those components in immunosorbent assay system they were able to cut the time necessary for analysis of s-IgA from 24 hours down to 1 hour[86].

It's important to note, that microfluidic immunosensors are devices are usually made of relatively inexpensive materials using simple fabrication methods. However, different and more sophisticated methods described above could be integrated for more sensitive detection of antibodies, rapid analysis of multiple analytes with small sample volumes, complex functionality with different mixers, dilutor networks and valves for separation, higher throughput with different surface chemistries, and specific binding via functionalization of the platforms with various hapten groups[87-90].

REFERENCES

70. Ekins RP. Immunoassay and other ligand assays: from isotopes to luminescence. J Clin Ligand Assay 1999;22:61– 77.

71. Lowe CR. Analytical biotechnology. Curr Opin Biotechnol 1996;7:1–3.

72. Aizawa M. Immunosensors. Bioprocess Technol 1991;15: 249–66.

73. Gizeli E, Lowe CR. Immunosensors. Curr Opin Biotechnol 1996;7:66–71.

74. Mahoney WC, Luderer AA, Brier RA, Lin JN. Real-time immunodiagnostics employing optical immunobiosensors. In: Chan DW, editor. Immunoassay automation. An updated guide to systems. San Diego: Academic Press; 1996.

75. Ghindilis AL, Atanasov P, Wilkins M, Wilkins E. Immunosensors: electrochemical sensing and other engineering approaches. Biosens Bioelectron 1998;13:113–31.

76. Pearson JE, Gill A, Vadgama P. Analytical aspects of biosensors. Ann Clin Biochem 2000;37:119–45.

77. Yang T, Jung S, Mao H, Cremer PS. Fabrication of phopholipid bilayer-coated microchannels for on-chip immunoassays. Anal Chem 2001;73:165–9.

78. Kaiser T, Gudat P, Stock W, Pappert G, Luppa PB. Biotinylated steroid derivatives as ligands for biospecific binding studies with monoclonal antibodies using immunosensor technology. Anal Biochem 2000;282:173–85.

79. Berney HC, Alderman J, Lane WA, Collins JK. Development of a capacitive immunosensor: a comparison of monoclonal and polyclonal capture antibodies as the primary layer. J Mol Recognit 1998;11:175–7.

80. Jiang, Xingyu, et al. "A miniaturized, parallel, serially diluted immunoassay for analyzing multiple antigens." Journal of the American Chemical Society125.18 (2003):

5294-5295.

81. Chen, H., Hughes, D. D., Chan, T. A., Sedat, J. W., and Agard, D. A. (1996) IVE (Image Visualization Environment): a software platform for all three-dimensional microscopy applications. J. Struct. Biol. 116, 56–60.

82. Paddock, Stephen W. "Principles and practices of laser scanning confocal microscopy." Molecular biotechnology 16.2 (2000): 127-149.

83. Diaspro, Alberto. "Confocal and two-photon microscopy: foundations, applications and advances." Confocal and Two-Photon Microscopy: Foundations, Applications and Advances, by Alberto Diaspro (Editor), pp. 576. ISBN 0-471-40920-0. Wiley-VCH, November 2001. (2001): 576.

84. Bromberg, A., Mathies, R.A., 2004. Multichannel homogeneous immunoassay for detection of 2,4,6-trinitrotoluene (TNT) using a microfabricated capillary array electrophoresis chip. Electrophoresis 25 (12), 1895–1900.

85. Wolf, M., Juncker, D., et al., 2004. Simultaneous detection of C-reactive protein and other cardiac markers in human plasma using micromosaic immunoassays and self-regulating microfluidic networks. Biosens. Bioelectron. 19 (10), 1193–1202.

86. Sato, K., Tokeshi, M., et al., 2000. Integration of an immunosorbent assay system: analysis of secretory human immunoglobulin A on polystyrene beads in a microchip. Anal. Chem. 72 (6), 1144–1147

87. Ng, J.M.K., Gitlin, I., et al., 2002. Components for integrated poly(dimethylsiloxane) microfluidic systems. Electrophoresis 23 (20), 3461–3473.

88. Yoshida, M., Shigemori, K., et al., 1993. Sensitivity enhancement of evanescent wave immunoassay. Measurement Sci. Technol. 4 (10), 1077–1079.

89. Ahn, C.H., Henderson, H.T., et al., 1998. Development of a generic microfluidic system for electrochemical immunoassay-based remote bio/chemical sensors. Proc. mTAS ’98, 225–230.

90. Becker, H., Locascio, L.E., 2002. Polymer microfluidic devices. Talanta 56 (2), 267–287.